AGU PUBLICATIONS

JGR

Journal of Geophysical Research: Atmospheres

RESEARCH ARTICLE
10.1002/2015JD023290

Key Points:
- Sublimation analysis was done on the Greenland NEEM ice core
- The major soluble salt particles are NaCl, Na_2SO_4, $CaSO_4$, and $CaCO_3$
- The fraction of primary aerosol is higher than that in inland Antarctica

Correspondence to:
I. Oyabu,
oyabu@lowtem.hokudai.ac.jp

Citation:
Oyabu, I., Y. Iizuka, H. Fischer, S. Schüpbach, G. Gfeller, A. Svensson, M. Fukui, J. P. Steffensen, and M. Hansson (2015), Chemical compositions of solid particles present in the Greenland NEEM ice core over the last 110,000 years, *J. Geophys. Res. Atmos.*, *120*, 9789–9813, doi:10.1002/2015JD023290.

Received 2 MAR 2015
Accepted 13 AUG 2015
Accepted article online 19 AUG 2015
Published online 28 SEP 2015

Chemical compositions of solid particles present in the Greenland NEEM ice core over the last 110,000 years

Ikumi Oyabu[1,2,3], Yoshinori Iizuka[1], Hubertus Fischer[4], Simon Schüpbach[4], Gideon Gfeller[4], Anders Svensson[5], Manabu Fukui[1], Jørgen Peder Steffensen[5], and Margareta Hansson[3]

[1]Institute of Low Temperature Science, Hokkaido University, Sapporo, Japan, [2]Graduate School of Environmental Science, Hokkaido University, Sapporo, Japan, [3]Department of Physical Geography, Stockholm University, Stockholm, Sweden, [4]Climate and Environmental Physics, Physics Institute and Oeschger Centre for Climate Change Research, University of Bern, Bern, Switzerland, [5]Centre for Ice and Climate, Niels Bohr Institute, University of Copenhagen, Copenhagen, Denmark

Abstract This study reports the chemical composition of particles present along Greenland's North Greenland Eemian Ice Drilling (NEEM) ice core, back to 110,000 years before present. Insoluble and soluble particles larger than 0.45 μm were extracted from the ice core by ice sublimation, and their chemical composition was analyzed using scanning electron microscope and energy dispersive X-ray spectroscopy and micro-Raman spectroscopy. We show that the dominant insoluble components are silicates, whereas NaCl, Na_2SO_4, $CaSO_4$, and $CaCO_3$ represent major soluble salts. For the first time, particles of $CaMg(CO_3)_2$ and $Ca(NO_3)_2{\cdot}4H_2O$ are identified in a Greenland ice core. The chemical speciation of salts varies with past climatic conditions. Whereas the fraction of Na salts ($NaCl + Na_2SO_4$) exceeds that of Ca salts ($CaSO_4 + CaCO_3$) during the Holocene (0.6–11.7 kyr B.P.), the two fractions are similar during the Bølling-Allerød period (12.9–14.6 kyr B.P.). During cold climate such as over the Younger Dryas (12.0–12.6 kyr B.P.) and the Last Glacial Maximum (15.0–26.9 kyr B.P.), the fraction of Ca salts exceeds that of Na salts, showing that the most abundant ion generally controls the salt budget in each period. High-resolution analyses reveal changing particle compositions: those in Holocene ice show seasonal changes, and those in LGM ice show a difference between cloudy bands and clear layers, which again can be largely explained by the availability of ionic components in the atmospheric aerosol body of air masses reaching Greenland.

1. Introduction

Aerosols are of central importance for atmospheric chemistry and physics, and climate [*Pöschl*, 2005]. Primary aerosols are emitted directly as liquid or solid particles from land or sea surface. On the other hand, secondary aerosols are formed by gas-to-particle conversion and chemical reactions in the atmosphere [*Hinds*, 1999]. During transport, all aerosols may undergo various physical and chemical interactions, changing their size, structure, and composition [*Pöschl*, 2005].

Aerosols may have an anthropogenic or natural source. Although it is now well recognized that anthropogenic activities have strongly modified the load and composition of aerosol in the present-day atmosphere, the composition of aerosols discussed in this study mainly originate from natural sources. Accordingly, we only deal with natural aerosols in this study. In the Arctic region, the natural soluble aerosols originate from the primary emission of sea salt (e.g., NaCl and $MgCl_2$) [e.g., *Legrand and Delmas*, 1988b; *Hansson*, 1994; *De Angelis et al.*, 1997; *Legrand and Mayewski*, 1997] and terrestrial materials (e.g., $CaSO_4$ and $CaCO_3$) [e.g., *Mayewski et al.*, 1994; *Hansson*, 1994; *De Angelis et al.*, 1997; *Legrand and Mayewski*, 1997]. Biomass burning plumes also represent a significant source of aerosol (e.g., KNO_3, K_2SO_4, and KCl) [e.g., *Popovicheva et al.*, 2014]. Soluble aerosol of the Arctic region is also secondarily produced from several sources, including NH_3 emitted by bacterial decomposition in soils and biomass burning [e.g., *Fuhrer et al.*, 1996; *Silvente and Legrand*, 1993; *Hansson and Holmén*, 2001; *Fischer et al.*, 2015], sulfur species emitted by marine biological activity (dimethyl sulfide (DMS)) and volcanoes (SO_2) [e.g., *Legrand and Delmas*, 1988b; *Hansson and Saltzman*, 1993; *Legrand et al.*, 1997; *Legrand and Mayewski*, 1997], and nitrogen oxides emitted from the surface soil by microorganisms and biomass burning or produced within the troposphere (lightning) and stratosphere (N_2O oxidation) [e.g., *Fuhrer and Legrand*, 1997; *Legrand and Mayewski*, 1997; *Röthlisberger et al.*, 2002]. Secondary aerosol contains salts such as NH_4NO_3, NH_4HSO_4, and $(NH_4)_2SO_4$.

Such atmospheric water-soluble aerosols are trapped and preserved in ice, representing important proxies to reconstruct past atmospheric environmental conditions [e.g., *Legrand*, 1995]. A useful technique for reconstructing past soluble aerosols from ice cores is the determination of the anions and cations, and this can be done either by ion chromatography [e.g., *Legrand et al.*, 1993, 1997; *Littot et al.*, 2002] or fluorescence and absorbance methods [*Röthlisberger et al.*, 2000; *Kaufmann et al.*, 2008; *Bigler et al.*, 2011]. Using ion concentrations, long-term aerosol studies have been done on Greenland ice cores from Dye 3 [*Hammer et al.*, 1985], Renland [*Hansson*, 1994], Greenland Ice Core Project (GRIP) [*Fuhrer et al.*, 1993; *De Angelis et al.*, 1997; *Legrand et al.*, 1997], Greenland Ice Sheet Project 2 (GISP2) [*Mayewski et al.*, 1994], and North Greenland Ice Core Project (NGRIP) [*Jonsell et al.*, 2007; *Ruth et al.*, 2007; *Bigler et al.*, 2011; *Fischer et al.*, 2015]. Concerning specific ions, the concentration of Ca^{2+}, a terrestrial proxy, decreases from cold to warm periods up to a factor of 80 between the Last Glacial Maximum (LGM; 15.0–26.9 kyr B.P.) and the Holocene in the GRIP and GISP2 ice cores [e.g., *Mayewski et al.*, 1994; *De Angelis et al.*, 1997; *Fischer et al.*, 2007]. The Na^+ concentration, a proxy of sea salt, varies less than Ca^{2+} but is still much more concentrated in cold periods than in warm periods [e.g., *Mayewski et al.*, 1994; *De Angelis et al.*, 1997; *Fischer et al.*, 2007]. The NH_4^+ concentration, originating mainly from continental biogenic emissions, starts to increase around Bølling-Allerød (12.9–14.6 kyr B.P.) from very low values in the last glacial period. Note that NH_4^+ is a major cation together with H^+ on a molar basis, whereas NH_4^+ dominates H^+ on a mass basis in the Holocene [*Hansson*, 1994; *Fuhrer and Legrand*, 1997; *Fuhrer et al.*, 1996; *Hansson and Holmén*, 2001]. The SO_4^{2-} concentrations are higher in cold periods than in warm periods [*Hansson*, 1994; *Legrand et al.*, 1997]. Whereas noneruptive volcanic emissions and marine biogenic emissions are the main sulfate sources during the Holocene [*Legrand et al.*, 1997], the large imbalance observed between cations and anions in LGM Greenland ice [*Legrand and Mayewski*, 1997] suggest that the strong increase of sulfate in glacial ice reflects increased terrestrial inputs (direct emissions of gypsum and $CaCO_3$ neutralized in the atmosphere by H_2SO_4).

Aerosols affect climate by direct and indirect effects [*Intergovernmental Panel on Climate Change*, 2007, 2013]. The effects of atmospheric aerosols on climate changes vary according to their concentration, size, structure, and chemical compositions [*Pöschl*, 2005]. Therefore, to determine the relevant chemical compositions of past atmospheric environments, one should determine not only the ion concentrations but also the chemical compositions of particles in the ice cores.

The first attempt to identify the chemical composition of soluble salts present in ice was done by measuring major anions and cations with ion chromatography, doing acidity measurements and examining the resulting ionic budget. This was done mainly in Antarctic ice [*Legrand*, 1987; *Legrand and Delmas*, 1988a]. Though no acidity measurements were available in Greenland ice from the LGM, an observed imbalance between major cations and anions measured with ion chromatography also provided some useful information on the association between anions and cations [*Legrand and Mayewski*, 1997]. Later, *Iizuka et al.* [2008] estimated that the major component of the soluble salts in the LGM at Dome Fuji in Antarctica is $CaSO_4$, whereas those in the Holocene are Na_2SO_4 and $MgSO_4$. Concerning the chemical compositions of single particles, particle compositions in Antarctic ice spanning several glacial cycles have been reconstructed using the micro-Raman method [*Ohno et al.*, 2005, 2006; *Sakurai et al.*, 2010, 2011] and the sublimation-energy dispersive X-ray spectroscopy (EDS) method [*Iizuka et al.*, 2009, 2012a, 2012b, 2013; *Oyabu et al.*, 2014]. Then, *Sakurai et al.* [2009], using micro-Raman spectroscopy, found that $CaSO_4$ is a primary soluble compound throughout the Holocene and the last glacial period in GRIP. They also found $CaCO_3$ particles in the last glacial period. However, direct measurements of particle compositions in the Greenland ice sheet remain rather sparse. Using the sublimation method, we present here the chemical compositions of major soluble and insoluble particles over the last 110,000 years before present (kyr B.P.) in the Greenland North Greenland Eemian Ice Drilling (NEEM) ice core.

2. Methods

2.1. Ice Core Sample

The NEEM ice core was drilled on the Northwestern Greenland ice sheet (77.45°N, 51.06°W; 2450 m above sea level) from 2007 to 2011. The core is 2540 m long and covers the past 130 kyr [*North Greenland Eemian Ice Drilling* (*NEEM*) *community members*, 2013]. The ice core samples applied in this study were transported from the field to the Niels Bohr Institute's (Denmark) cold storage facility and afterward to a cold laboratory at the

Department of Physical Geography, Stockholm University (Sweden), where they were kept frozen at −25°C. In the NEEM core, stratigraphic disruptions exist below the 2209.60 m depth [*NEEM community members*, 2013], and for this study samples have been selected from the section above 2200 m. The applied NEEM ice core timescale is from *Rasmussen et al.* [2013]. We refer to the NEEM water isotope profile (unpublished) to select 86 sections from six different climatic stages. The stages follow the Greenland interstadials (GI) and Greenland stadials (GS) described in *Rasmussen et al.* [2014] such that 26 sections are from the Holocene (0.9–11.7 kyr B.P.), 3 sections are from the Younger Dryas (YD; GS-1, 12.0–12.6 kyr B.P.), 7 sections are from the Bølling Allerød (BA; GI-1, 12.9–14.6 kyr B.P.), 20 sections are from the LGM (GS-2 and GS-3, 15.0–26.9 kyr B.P.), 17 sections are from interstadial periods of Dansgaard-Oeschger (DO) event (GI-3 to GI-24), and 13 sections are from stadial periods of DO event (GS-4 to GS-22) (Table 1).

The NEEM isotope data are not available yet, but the overall features are very similar to those of the North Greenland Ice Core Project (NGRIP) isotope data [*Montagnat et al.*, 2014]. A chronology for the NEEM ice core has been derived by transferring the annual layer count in the Greenland Ice Core Chronology 2005 (GICC05) and its model extension (GICC05modelext) from the NGRIP core to the NEEM core [*Rasmussen et al.*, 2013]. Thus, we used the NGRIP water isotope profile [*Rasmussen et al.*, 2014] as a reference of the temperature changes also at NEEM.

The ion and dust concentrations were analyzed using the continuous flow analysis (CFA) system of the University of Bern [*Kaufmann et al.*, 2008]. The Ca^{2+} and Na^{+} concentrations of 50 bag means (i.e., 55 cm resolution) from 1282.5 to 1629.65 m are shown in Figure 13; and dust, Ca^{2+}, Na^{+}, NH_4^{+}, and NO_3^{-} from an early Holocene section (1302.95–1303.50 m) and from a LGM section (1555.95–1556.50 m) in 1 mm resolution are shown in Figures 14 and 15, respectively.

2.2. Observation of Nonvolatile Particles by Sublimation-EDS Method

To extract the nonvolatile particles, we followed the procedure described in *Iizuka et al.* [2009]. The sublimation system used in this study is placed at the Stockholm University, Sweden. We decontaminated the ice samples by shaving about 1–2 mm off the surface using a clean ceramic knife and pulverized about 1 g of ice from the deepest 5 cm of each of a 55 cm section of the core. The pulverized ice was then placed on a polycarbonate membrane filter (diameter 13 mm, pore size 0.45 μm) in a sublimation chamber cooled to −40°C. Dry, clean air with a compression air pressure of 0.55 MPa, containing no oil or solid particles more than 0.03 mm in diameter flowed through the chamber at a rate of 15 L min^{-1} for 50 h. The air was produced by an air compressor (Hitachi oil-free Bebicon, 0.75OP-9.5GS5/6), an air dryer, and a cleaner (SMC Coop. IDG60SV). Each filter yielded more than 700 particles exceeding 0.45 μm diameter. Constituent elements and particle diameter were measured using a JSM-6360LV (Japan Electron Optics Laboratory) SEM (scanning electron microscope) and a JED2201 (JEOL) EDS (energy dispersive X-ray spectroscopy) system at the Institute of Low Temperature Science (ILTS), Hokkaido University, Japan. To avoid electrical charging of the filter and to improve analysis accuracy, the filter was coated with a Pt film by magnetron sputtering (MSP-10 Magnetron Sputter) before the SEM-EDS measurement. The accelerating voltage was 20 keV with a working distance of 20 mm and a collecting time of 30–60 s. To be counted as a nonvolatile particle, a particle had to contain at least one of the elements Na, Mg, Si, Al, S, Cl, K, and Ca, each with an atomic ratio (%) amount at least twice that of the error (%). The elements C, Cr, Fe, and Pt were also observed but not used in the analyses because their signal could not be distinguished from artifacts from the membrane filter (C), the sample mount (Cr), the stainless steel of the sublimation system (Fe), and the filter coating (Pt). Other elements were only rarely detected.

To evaluate possible contamination during the sublimation process, the sublimation system was run twice before setting the ice sample on the filter in the sublimation chamber. After flowing air for 100 h, the filter was observed by the SEM-EDS. As a result, only three to five particles with C and O were found. As each ice sample would leave behind more than several thousand particles for glacial samples and 700 particles for Holocene sample, the three to five particles not from the ice constitute less than 1%. Moreover, as particles containing only C and O are not counted as nonvolatile particles here, we conclude that contamination from the sublimation system is not an issue.

The analyzed salt particles were likely solid when embedded in the ice sheet, but possibly in the upper 10 m and in the lower half of the core, some salts such as NaCl may have been liquid. The eutectic temperature is −21.3°C for NaCl [*Usdowski and Dietzel*, 1998], whereas those of $CaCO_3$, $CaSO_4$, and Na_2SO_4 are close to zero [*Kargel*, 1991; *Usdowski and Dietzel*, 1998]. The mean annual temperature at NEEM is −29°C

Table 1. Overview of the NEEM Ice Core Sections Used for This Study[a]

Depth (m)	Age (kyr B.P.)	Climate Stage	Number of Measured Particles	Mean Diameter (μm)
219.45	0.9	Holocene	574	1.05
376.75	1.7	Holocene	669	2.23
441.65	2.1	Holocene	585	2.40
544.50	2.7	Holocene	518	2.18
665.50	3.4	Holocene	476	1.60
689.15	3.6	Holocene	662	2.25
1282.60	8.9	Holocene	309	2.11
1289.75	9.0	Holocene	301	2.40
1296.90	9.2	Holocene	300	2.22
1303.50	9.3	Holocene	307	1.96
1311.20	9.4	Holocene	304	3.22
1319.45	9.5	Holocene	299	2.33
1326.60	9.6	Holocene	306	2.43
1333.20	9.8	Holocene	315	1.82
1340.35	9.9	Holocene	293	1.91
1346.95	10.0	Holocene	305	2.64
1354.10	10.2	Holocene	306	2.73
1360.15	10.3	Holocene	312	1.92
1367.85	10.4	Holocene	271	3.15
1374.45	10.6	Holocene	307	1.82
1382.15	10.8	Holocene	301	2.83
1388.75	10.9	Holocene	313	2.50
1395.90	11.1	Holocene	307	2.00
1402.50	11.3	Holocene	313	2.26
1409.65	11.5	Holocene	298	1.99
1417.35	11.7	Holocene	306	2.27
1424.50	12.0	YD (GS-1)	305	2.00
1431.10	12.3	YD (GS-1)	309	2.06
1437.70	12.6	YD (GS-1)	307	2.07
1444.85	12.9	BA (GI-1)	301	2.24
1452.00	13.2	BA (GI-1)	333	3.14
1459.15	13.5	BA (GI-1)	306	2.20
1464.65	13.7	BA (GI-1)	309	2.25
1472.90	14.1	BA (GI-1)	305	1.95
1479.50	14.3	BA (GI-1)	268	2.73
1486.65	14.6	BA (GI-1)	329	2.42
1493.25	15.0	LGM (GS-2)	306	1.93
1500.40	15.5	LGM (GS-2)	272	3.02
1501.50	15.6	LGM (GS-2)	515	1.33
1508.10	16.1	LGM (GS-2)	301	2.06
1515.25	16.7	LGM (GS-2)	300	1.87
1517.45	16.8	LGM (GS-2)	738	1.64
1522.40	17.2	LGM (GS-2)	305	2.29
1529.00	17.7	LGM (GS-2)	312	1.82
1536.15	18.2	LGM (GS-2)	308	2.94
1540.00	18.5	LGM (GS-2)	732	1.95
1543.85	18.8	LGM (GS-2)	307	2.59
1551.00	19.4	LGM (GS-2)	304	2.35
1556.50	19.8	LGM (GS-2)	539	4.46
1558.15	19.9	LGM (GS-2)	309	2.01
1564.75	20.5	LGM (GS-2)	301	2.98
1571.90	21.0	LGM (GS-2)	306	1.87
1573.00	21.1	LGM (GS-2)	735	1.66
1578.50	21.6	LGM (GS-2)	304	2.47
1622.50	26.1	LGM (GS-3)	737	1.79
1630.20	26.9	LGM (GS-3)	763	2.15
1640.10	27.7	GI-3	531	1.99
1646.70	28.3	GS-4	741	1.73
1652.20	28.8	GI-4	528	1.38
1669.25	30.6	GS-5.1	536	1.44
1687.40	32.3	GI-5.2	515	1.26

Table 1. (continued)

Depth (m)	Age (kyr B.P.)	Climate Stage	Number of Measured Particles	Mean Diameter (μm)
1695.10	33.1	GS-6	615	1.64
1700.60	33.6	GI-6	529	1.46
1708.30	34.3	GS-7	528	1.63
1718.20	35.2	GI-7	511	1.19
1727.00	35.9	GS-8	515	1.45
1757.25	38.1	GI-8	301	2.02
1765.50	38.8	GS-9	307	2.23
1790.25	41.4	GI-10	303	2.02
1795.75	41.9	GS-11	304	2.23
1808.95	43.2	GI-11	221	2.04
1811.70	43.5	GS-12	309	2.13
1844.70	46.7	GI-12	310	1.98
1852.95	47.7	GS-13	304	2.06
1888.70	51.9	GI-14	306	1.86
1925.00	56.0	GS-16.1	303	2.16
1942.60	58.3	GI-16.2	307	2.04
1963.50	61.5	GS-18	308	2.23
1986.60	66.8	GS-19.1	308	1.97
2010.25	72.3	GI-19.2	307	2.19
2063.60	81.9	GI-21.1	305	1.87
2096.60	86.0	GS-22	303	2.34
2128.50	90.0	GI-22	306	2.12
2137.85	91.5	GI-23.1	303	2.12
2180.20	101.4	GI-23.1	282	2.11
2195.60	106.7	GI-24.1	300	1.98

[a]The event stratigraphies divide the characteristic sequence of Greenland climate changes in the glacial period into numbered Greenland interstadials (GI) and Greenland stadials (GS) following *Rasmussen et al.* [2014].

[*NEEM community members*, 2013], which means that in summer at the surface and in the lower half of the core, the in situ temperature may exceed the eutectic temperature of NaCl. When the air temperature exceeds −21.3°C, NaCl may precipitate as a liquid and then spread or remain as a droplet on the snow surface. However, NaCl become solid when it buried in the depth of 10 m, where the temperature should be around −29°C at NEEM. Although the temperature of ice increases at greater depths in the core, being below the close-off depth ensures that the NaCl remains confined and later precipitates back to solid form in the −25°C cold room. Thus, we do not consider liquid-phase processes in our analyses of the salt particles.

On the other hand, H_2SO_4 is expected to be present as liquid in the ice sample and during sublimation (the eutectic temperature is −62.0°C [*Marion*, 2002]), but H_2SO_4 should not affect the particles during sublimation [*Oyabu et al.*, 2014]. As a way to check salt sulfatization during sublimation, *Oyabu et al.* [2014] compared the number ratio of $Na_2SO_4/CaSO_4$ from the sublimation method to that from the micro-Raman method. The micro-Raman directly determined the amounts of both compounds preserved in the ice, from which we obtained the ratio. The resulting ratio from both methods agreed with each other, suggesting that chemical reactions between acids and salts are unlikely during the sublimation process.

In total, 32,867 particles from 86 ice samples were analyzed. Of all the particles on a given filter, about 300–500 were chosen at random to analyze, averaging in 380 particles/sample. The major diameters of the particles were measured. Aggregate particles such as those shown in Figure 1a are regarded as multiple particles, and particles such as those shown in Figures 1b–1e are regarded as single particles. The mean diameters of the particles analyzed in each sample are listed in Table 1. The mean diameter of all 32,867 analyzed particles is 2.08 ± 0.46 μm. Our study focuses on the compositions of particles originating from terrestrial material and sea salt, including their secondary aerosols, particles that occur mainly in coarse particle mode (>1 μm) [*Whitby*, 1978]. Therefore, the mean diameters of the particles measured in this study are consistent with particles that originate from terrestrial material and sea salt.

The mole numbers of $CaCO_3$, $CaSO_4$, Na_2SO_4, NaCl, Ca-Cl, and NaX were calculated for each sample using the spectrum ratios of each element obtained by SEM-EDS. The calculation procedure for the calculation of moles and their uncertainties are explained in Appendix A.

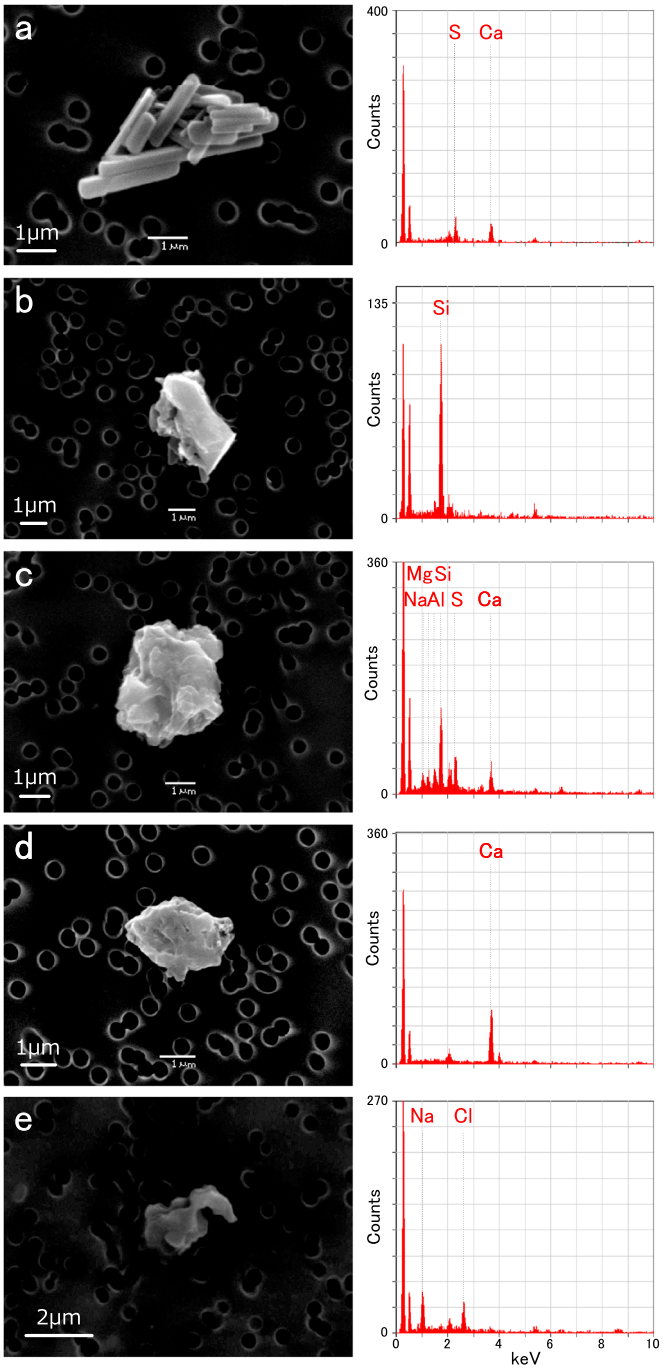

Figure 1. SEM images of representative particles from 13.5 kyr B.P. (a) Particle containing Ca and S. (b) Particle containing Si. (c) Particle containing Na, Mg, Al, Si, S, and Ca. (d) Particle containing Ca. (e) Particle containing Na and Cl. The left peak is C (artifact from the filter), the peak second from the left is O, and the peak near 2.0 keV is Pt (artifact from the coating).

2.3. Separating the Soluble and Insoluble Components

To separate the nonvolatile particles into soluble and insoluble components, we ran water immersion experiments on the Holocene (2.7 kyr B.P.) and the LGM (19.8 kyr B.P.) sections by following the procedure described by *Iizuka et al.* [2009]. After extracting the nonvolatile particles, their elemental compositions were measured using SEM-EDS without a Pt film coating. Then the water-soluble particles were dissolved by continually putting an ultrapure water drop on the filter at 25°C for 24 h, and letting each drop pass through the filter. Thus, particles do not float and get away from filter. After drying, the filter was coated by a Pt film, and then the residue of insoluble particles remaining on the filter was analyzed once more using SEM-EDS. In this way, we could measure the elemental compositions of nonvolatile and insoluble particles from the same sample. From the Holocene section, 518 nonvolatile particles and 218 insoluble particles were analyzed. From the LGM section, 539 nonvolatile particles and 232 insoluble particles were analyzed. After considering the possible remaining combination of elements, we classified the nonvolatile particles into insoluble and soluble particles.

2.4. Micro-Raman Spectroscopy of the Calcium Compounds

A certain amount of soluble Ca-containing particles was observed during the SEM-EDS measurement. To determine the compositions of such soluble Ca-containing particles, we analyzed particles extracted by sublimation system using micro-Raman spectroscopy, and then the same particles were measured by SEM-EDS. Glacial ice from 19.8 kyr B.P. and 28.3 kyr B.P. was selected. A $5 \times 5 \times 1\ mm^3$ Cr plate was mounted to a membrane filter before placing the ice sample in the sublimation chamber. Then about 1 g of pulverized ice sample was placed on the Cr plate, and volatile materials were sublimated at −40°C as described in section 2.2. A total of 223 particles from the 19.8 kyr B.P. sample and 200 particles from the 28.3 kyr B.P. sample were analyzed by micro-Raman spectrometer at ILTS (Japan). The micro-Raman spectrometer at ILTS has a triple monochromator (Jobin-Yvon, T64000) equipped with a charge-coupled device (CCD) detector (Jobin-Yvon, Spectraview-2D). Laser light of wavelength 514.5 nm and power 150 mW was focused on a particle for 60 s. To identify the

Table 2. Sample List of High-Resolution Analysis

Sample Name	Layer	Depth (m)	Age (kyr B.P.)	Number of Measured Particles
LGM-01	clear layer	1556.00	19.8	208
LGM-02	cloudy band	1556.13		524
LGM-03	clear layer	1556.17		510
LGM-04	cloudy band	1556.22		511
LGM-05	clear layer	1556.25		514
Holocene-01	winter	1303.18	9.3	206
Holocene-02	summer	1303.24		202
Holocene-03	spring	1303.30		200
Holocene-04	summer	1303.35		198

chemical compositions of particles, the observed spectra were compared with those of reference specimens, which included $CaCO_3$ (Kishida Chemical), $Ca(NO_3)_2{\cdot}4H_2O$ (Wako Pure Chemical Industries), and $CaSO_4{\cdot}2H_2O$ (Kishida Chemical). For dolomite ($CaMg(CO_3)_2$), we referred to spectra from an open database [*Downs*, 2006]. After the micro-Raman analysis, the elemental compositions of nonvolatile particles of the same plates were measured by SEM-EDS. We collected data from 208 particles from the 19.8 kyr B.P. section and 206 particles from the 28.3 kyr B.P. section by the SEM-EDS measurement.

2.5. Sublimation-EDS Analysis at Centimeter Resolution

The soluble salt analyses at centimeter-scale resolution are useful to investigate variations at the seasonal scale. To understand the chemical compositions of soluble salt particles with higher resolution, we examine centimeter-scale measurements on selected sections from the LGM (1555.95–1556.50 m; 19.8 kyr B.P.) and from the Holocene (1302.95–1303.50 m; 9.3 kyr B.P.) (Table 2).

All glacial Greenland ice cores are revealing bands of cloudy and clear ice [e.g., *Meese et al.*, 1997; *Shimohara et al.*, 2003]. Annual layers will appear as single or multiple visible layers in the cloudy bands and clear layers. Thus, the change from cloudy to clear bands is not always related to seasonal change [*Svensson et al.*, 2005]. From visual observation, five layers of 1 cm thickness were selected from the LGM section, hereafter denote LGM-01 to LGM-05. Samples LGM-01, LGM-03, and LGM-05 are from clear layers (1560.00, 1556.17, and 1556.25 m), whereas LGM-02 and LGM-04 (1556.13 and 1556.22 m) are from cloudy bands known from previous studies [e.g., *Ram and Koenig*, 1997; *Svensson et al.*, 2005] to have high dust and Ca^{2+} concentrations (Table 2).

In the Holocene ice, the level of impurities remains far lower than that reached during the LGM, and thus, no cloudy bands have been detected. Yet the Holocene ice has seasonal ion variations; for example, the dust and Ca^{2+} are of terrestrial origin and peak in spring [e.g., *Whitlow et al.*, 1992; *Kuramoto et al.*, 2011; *Gfeller et al.*, 2014], whereas the Na^+ originates from sea salt and peaks in winter, and the NO_3^- and NH_4^+ that originate mainly from bacterial decomposition and biomass burning, peak in the summer [*Whitlow et al.*, 1992; *Fuhrer et al.*, 1996; *Legrand and Mayewski*, 1997; *Kuramoto et al.*, 2011]. Apart from volcanism, the natural source of SO_4^{2-} is from DMS emission from marine biogenic activity and continental biogenic emissions that peaks in summer [*Kuramoto et al.*, 2011]. Based on the CFA records, we selected four layers from the Holocene section, hereafter Holocene-01 to Holocene-04. Holocene-01 has a Na^+ peak (1303.18 m), Holocene-02 has NH_4^+ and NO_3^- peaks (1303.24 m), Holocene-03 has dust and Ca^{2+} peaks (1303.30 m), and Holocene-04 has NH_4^+ and NO_3^- peaks (1303.35 m) (Table 2). Given their peaks, we assume that Holocene-01 is a winter layer, Holocene-02 and Holocene-04 are summer layers, and Holocene-03 is a spring layer.

The ice samples were cut by hand saw and shaved with a ceramic knife for decontamination of the target layer. Then we put several millimeters of the target layer in the sublimation chamber for analysis. Each sample involved analyzing about 200–500 particles (Table 2).

3. Results and Discussion

3.1. Soluble and Insoluble Components of the NEEM Ice Core Samples

The nonvolatile particles exhibit various shapes. Needle-like particles, such as that in Figure 1a, are common in NEEM samples but rarely seen in Antarctic Dome Fuji samples. They are similar to SEM images of gypsum [e.g., *Badens et al.*, 1999] and, as they contain Ca and S, are likely to consist mainly of gypsum. However,

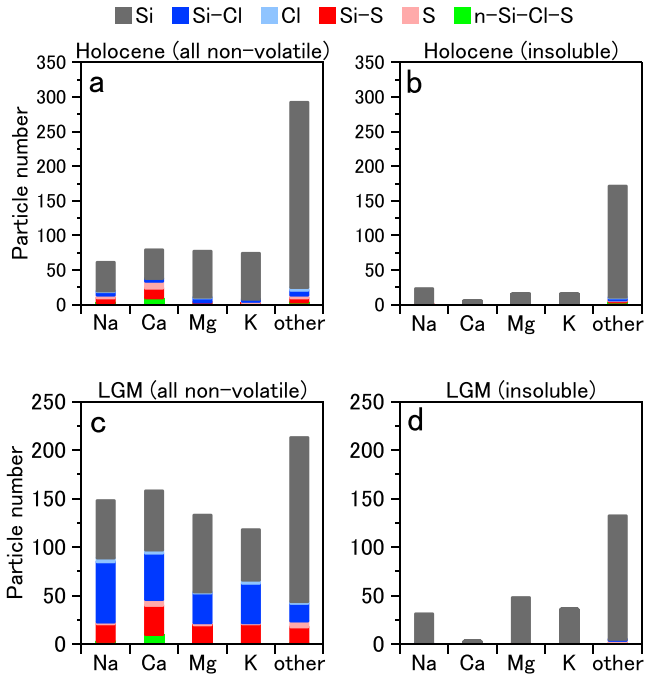

Figure 2. Number distribution of the elemental compositions of nonvolatile particles and insoluble particles from the Holocene section (2.7 kyr B.P.) and the LGM section (19.8 kyr B.P.). (a) The total nonvolatile particles from the Holocene section (before water immersion). (b) The insoluble particles from the Holocene section (after water immersion). (c) The total nonvolatile particles from the LGM section (before water immersion). (d) The insoluble particles from the LGM section (after water immersion). The bars depict Na-, Ca-, Mg-, and K-containing particles; "other" particles are particles without Na, Ca, Mg, and K. The colors depict the combination of Si-, S-, and Cl-containing particles according to the color legend above the chart. For example, green sections indicate particles containing no Si, Cl, or S.

particles containing Ca and S are not always needle shaped. They may, as those shown in Figures 1b–1d, contain other elements and have different shapes. Therefore, it is difficult to identify the particle compositions based on the shape alone. The samples in Figures 1b–1e are considered to be a silicate mineral (b), a mixture of silicate mineral and sulfate salt (c), a Ca compound (d), and a NaCl mineral (e).

Figures 2a and 2c show the total nonvolatile particles, which include both soluble and insoluble particles, whereas Figures 2b and 2d show insoluble particles. By comparing with Figures 2a and 2c and Figures 2b and 2d, one can see that almost all of the insoluble particles of both the Holocene (2.7 kyr B.P.) and the LGM (19.8 kyr B.P.) sections contain Si. As the major group of insoluble dust in the Greenland ice core are silicates [*Maggi*, 1997; *Svensson et al.*, 2000], we assume that Si-containing particles contain silica minerals. Of both sections, the total nonvolatile particles contain some S or Cl (Figures 2a and 2c), whereas the insoluble particles rarely contain S or Cl (Figures 2b and 2d). A particle containing S or Cl is considered to be a soluble compound. As sulfate and chloride are abundant in Greenland ice cores and as the concentration of MSA remains well below that of sulfate [*Hansson*, 1994; *Mayewski et al.*, 1994; *Legrand and Mayewski*, 1997; *Legrand et al.*, 1997], then the soluble S or Cl are probably components of sulfate or chloride salts.

We also checked components of Na, Ca, Mg, and K. By comparing to the total nonvolatile particles to the insoluble particles (remaining after water immersion), most of the Na-, Mg-, and K-containing particles lost the S, Cl, and n-Si-Cl-S (no Si, Cl, and S) components during dissolution, whereas the Si did not dissolve. On the other hand, the Ca-containing particles deplete significantly not only S, Cl, and n-Si-Cl-S components but also Si component. This result suggests that almost all Ca particles are water soluble.

3.2. Chemical Composition and Characteristics of Nonvolatile Particles

In this section, we examine particles from all samples. Consider the particles containing combinations of sulfate or chloride. Figure 3 shows 32,867 nonvolatile particles sorted into eight categories based on their content of Si (silicate dust), Cl (chloride salts), and S (sulfate salts). The Si-containing particles compose 85.7% of the total particles. The chloride salts (Cl- and Si-Cl particles) compose 17.8% of the total particles the sulfate salts (S- and Si-S particles) account for 18.1% of all particles, and the mixed salts of chloride and sulfate (Cl-S- and Si-Cl-S particles) account for 8.5% of all particles. More than 70% of these soluble salt particles include Si. The Si-Cl particles are likely a mixture of chloride salts and silicate dust. Such mixed particles are formed in the atmosphere when dust particles enter a marine-dominated atmosphere [*Zhang and Iwasaka*, 2001]. The Si-S particles may be mixture of silicate and sulfate salt, and the Si-Cl-S particle may be a mixture of silicate, chloride salt, and sulfate salt. Such particles may have interacted with other particles or compounds during atmospheric transport. Of the soluble particles, 92.1% contain chloride and sulfate salts. The numbers of chloride and sulfate salts are almost equal, showing that both sulfate and chloride salts are the major soluble salts in the NEEM ice core over the last 110 kyr.

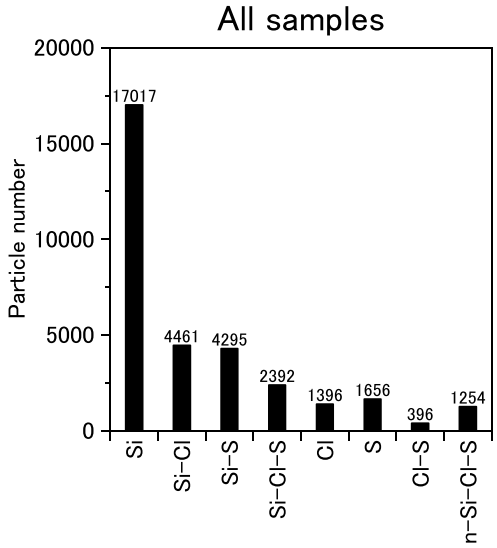

Figure 3. Number distribution of Si, Cl, and S particles from all samples. The bars depict combination of Si-, S-, and Cl-containing particles. For example, particles containing Si but not S and Cl are categorized in the Si bar. This bar indicates silicate dust. The Si-Cl bar indicates a mixture of chloride salts and silicate dust. The Si-S bar indicates a mixture of sulfate salts and silicate dust. The Si-Cl-S bar indicates a mixture of chloride salts, sulfate salts, and silicate dust. The Cl bar indicates chloride salts. The S bar indicates sulfate salts. The Cl-S bar indicates a mixture of chloride and sulfate salts. The n-Si-Cl-S bar indicates particles other than chloride salts, sulfate salts, and silicate dust.

Next, eight particle categories were examined based on their content of Na, Ca, Mg, and K (Figure 4). About half of the particles in the Si category contain no Na, Ca, Mg, and K (Figure 4a). This implies that the Si particles mainly consist of quartz, the most common silica mineral [*Maggi*, 1997], or kaolinite. Similar results for major components of insoluble silicate minerals were reported by *Maggi* [1997] and *Svensson et al.* [2000] in glacial Greenland ice. The most abundant element in the Cl category is Na (Figure 4b), most likely in the form of sea salt. Also, the most abundant element in the Si-Cl category is Na (Figure 4c). Thus, the most dominant chloride salt in NEEM is NaCl. For the S category, the most abundant element is Ca, with the second most abundant being Na (Figure 4d). The S-Ca combination indicates a $CaSO_4$ particle, and the S-Na combination is likely from Na_2SO_4. The presence of $CaSO_4$ in Greenland ice can be attributed to the primary emissions of gypsum and/or emissions of $CaCO_3$ then reacts with sulfuric acid following the reaction (1) ($CaCO_3 + H_2SO_4 \rightarrow CaSO_4 + CO_2 + H_2O$) [*Legrand et al.*, 1997]. The presence of Na_2SO_4 in polar ice is related to its production from sea salt during acidification following the reaction (2) ($2NaCl + H_2SO_4 \rightarrow Na_2SO_4 + 2HCl$) [*Legrand and Delmas*, 1988b]. In the Si-S category, the most abundant element is Ca, with the second most abundant being Na (Figure 4e). Thus, the most dominant sulfate salt is $CaSO_4$, and the second most dominant is Na_2SO_4. If a particle contains Ca, Na, and S, this particle was counted as both $CaSO_4$ and Na_2SO_4.

In the n-Si-Cl-S (no Si, Cl, and S) category, the most abundant element is Ca (Figure 4f). Compounds of such particles cannot be determined from SEM-EDS analysis, but as we will discuss in section 3.3, such Ca particles may be $CaCO_3$ or $Ca(NO_3)_2$ particles of terrestrial origin.

The Si-Cl, Si-S, and Si-Cl-S categories (Figures 4c, 4e, and 4h) are more likely to contain multiple elements of Na, Mg, Ca, and K than particles without Si (i.e., Cl, S, and Cl-S categories) (Figures 4b, 4d, and 4g). They are likely mixtures of chloride/sulfate salts and silicate dust. The proportion of particles in the Si-Cl category that have not only Na but other elements as well (Mg, Ca, and K) is higher than that in the Cl category. Similarly, that of Si-S particles having not only Ca but other elements as well is higher than that in the S category. The proportion of particles in the Si-Cl-S category having multiple elements is higher than that for Si-Cl and Si-S categories (Figure 4h). Such a composition mix indicates that the particles have interacted with other compounds such as silicate, H_2SO_4 [e.g., *Legrand and Delmas*, 1988b], NaCl [e.g., *Legrand and Delmas*, 1988b], KCl [e.g., *Popovicheva et al.*, 2014], $CaSO_4$, and/or $CaCO_3$ [e.g., *Legrand and Mayewski*, 1997] during atmospheric transport.

Particles without Si and particles containing Ca can be considered as soluble salt particles. The Ca salts ($CaX + CaSO_4$ + Ca-Cl particle) and Na salts ($NaCl + Na_2SO_4 + NaX$) account for 89.2% of the total soluble salt particles (Figure 5), making these salts the major soluble salts present in the NEEM ice. The Ca salts consist mainly of $CaSO_4$ and Ca particles without S or Cl (CaX), both types of which are probably of terrestrial origin. The Na salts consist mainly of NaCl and Na_2SO_4, which are probably mainly of sea-salt origin. Our interpretation, shown in Figure 5, is that the major soluble salt particles over the 110 kyr in the NEEM ice core are Ca particles without S or Cl (CaX), $CaSO_4$, NaCl, and Na_2SO_4.

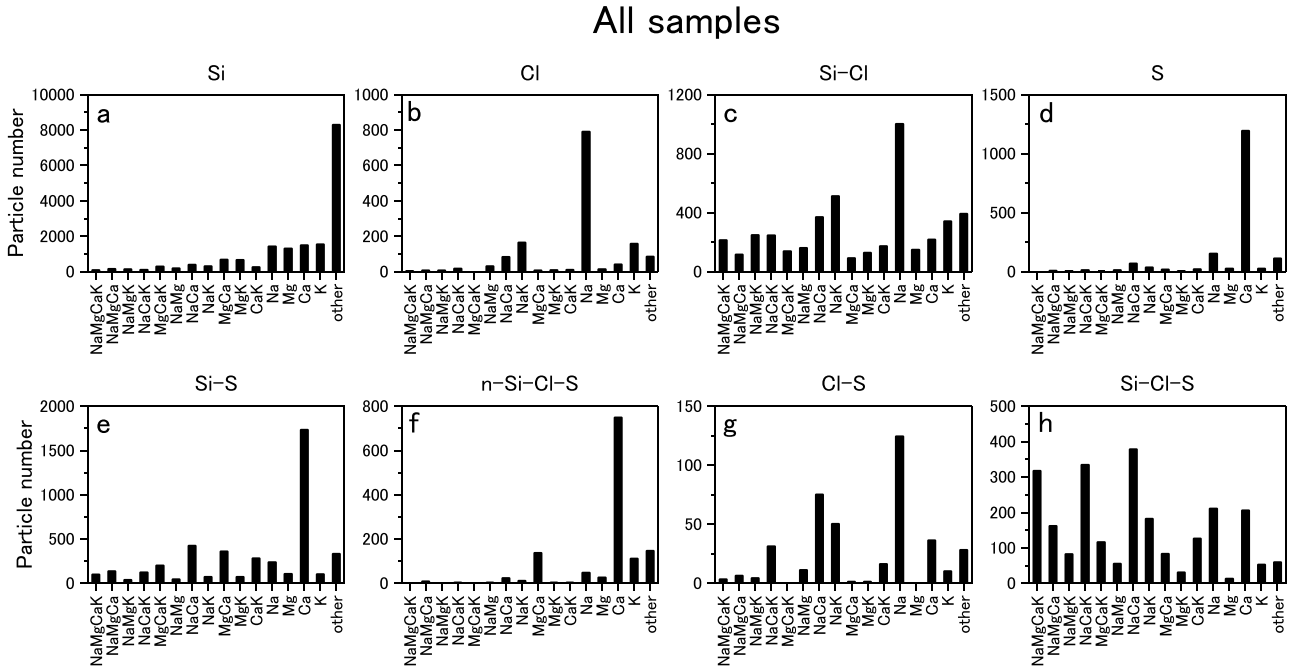

Figure 4. Number distribution of Si, Cl, and S particles focusing on Na, Mg, Ca, and K. Each panel gives the elemental compositions of Si, Cl, and S particles shown in Figure 3. The bars depict the particular combinations of Na-, Mg-, Ca-, and K-containing particles. For example, the NaMgCaK bar indicates particles containing Na, Mg, Ca and K. The Other bar indicates particles containing no Na, Mg, Ca, or K.

3.3. Identification of Calcium-Containing Particles by Micro-Raman Spectroscopy

Carbonates, such as $CaCO_3$, form a major component of mineral dust and are known to be reactive with H_2SO_4 and HNO_3 [*Liu et al.*, 2008]. It has been suggested that $CaCO_3$ and $Ca(NO_3)_2$ are deposited on the Greenland ice sheet [e.g., *Mayewski et al.*, 1994; *De Angelis et al.*, 1997; *Röthlisberger et al.*, 2002]. Later, *Sakurai et al.* [2009] identified $CaCO_3$ in the GRIP ice core. As noted above, we found a high amount of soluble Ca particles other than $CaSO_4$ (CaX); but the composition is still unclear. To determine the chemical compounds of "CaX," we analyzed particles using the micro-Raman spectroscopy, and then the same particles were measured by SEM-EDS.

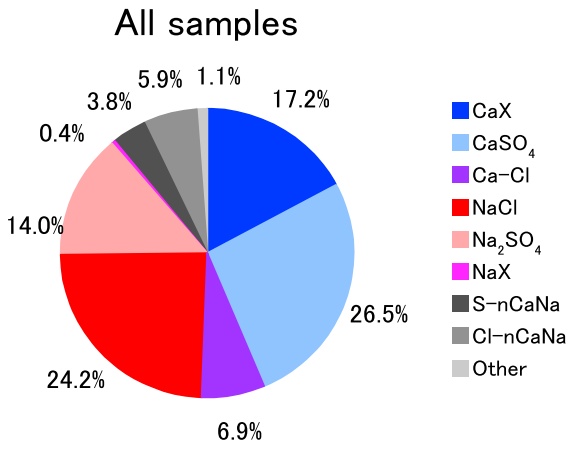

Figure 5. Number fraction of soluble components of all particles. CaX indicates particles containing Ca but neither S nor Cl. Ca-Cl indicates particles containing Ca and Cl. Since the eutectic temperature of $CaCl_2$ is low (approximately −50°C), it is not certain that such salt can be measured by the sublimation method. Therefore, we call particles containing Ca and Cl as Ca-Cl rather than $CaCl_2$. NaX indicates particles containing Na but no Si, S, or Cl. S-nCaNa indicates sulfate salts other than Na_2SO_4 and $CaSO_4$. Cl-nCaNa indicates chloride salts other than NaCl and Ca-Cl particles. Other indicates soluble salts other than sulfate and chloride salts. These nine categories cover all soluble salt particles.

The nonvolatile particles produced several sharp Raman peaks. Figure 6 shows the spectra from four particles with distinct spectra. To identify the species, we match their spectra to reference spectra and show the match just below the sample spectra. The reference specimen of $CaCO_3$ (Figure 6a) has a major peak at 1086 cm^{-1} (from the C–O symmetric stretching mode) and a secondary peak at 712 cm^{-1} from other modes, both of which match the particle sample. The reference $CaMg(CO_3)_2$ (dolomite) has a major peak at 1095 cm^{-1} (from the C–O

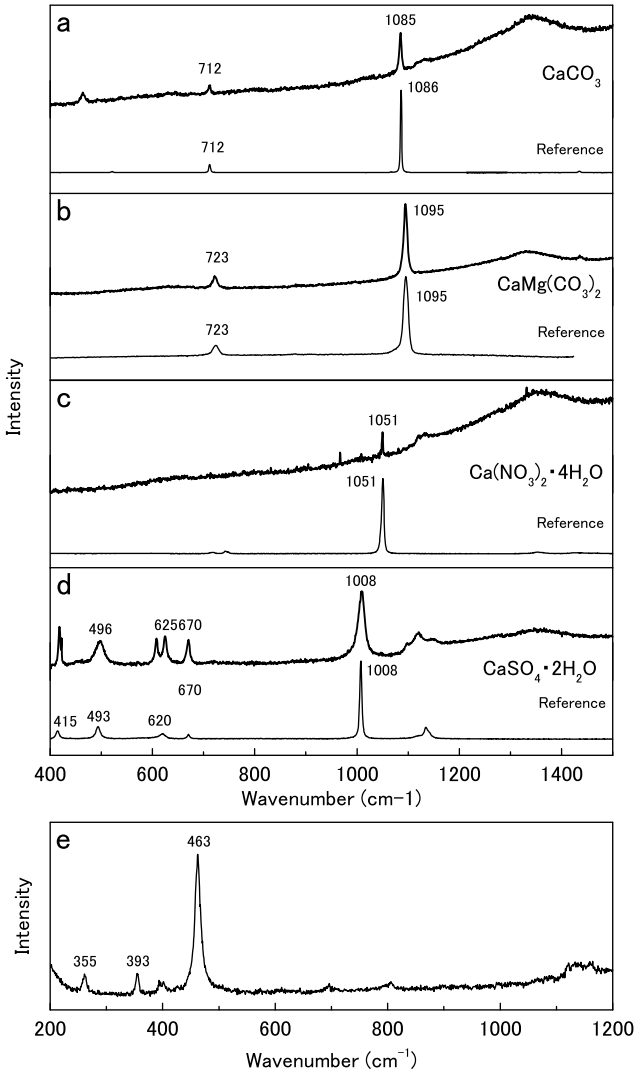

Figure 6. Raman spectra. Each panel shows observed spectra of nonvolatile particles of the LGM sections (top line) and reference data of the labeled compound (bottom line). (a) $CaCO_3$. (b) $CaMg(CO_3)_2$ (dolomite). (c) $Ca(NO_3)_2{\cdot}4H_2O$. (d) $CaSO_4{\cdot}2H_2O$. (e) Example of silicate mineral.

symmetric stretching mode) and a secondary peak at 723 cm^{-1}, both peaks matching the particle in Figure 6b. The reference $Ca(NO_3)_2{\cdot}4H_2O$ has a main peak at 1051 cm^{-1} (from the N–O symmetric stretching mode) that matches the particle in Figure 6c. The reference $CaSO_4{\cdot}2H_2O$ has a major peak at 1008 cm^{-1} (from the S–O symmetric stretching mode) and secondary peaks at 415, 493, 620, and 670 cm^{-1}, all peaks of which match peaks in the particle sample in Figure 6d. Thus, the spectra clearly show that $CaCO_3$, $CaMg(CO_3)_2$, $Ca(NO_3)_2{\cdot}4H_2O$, and $CaSO_4{\cdot}2H_2O$ are present in the glacial sections of the NEEM ice core, the $CaMg(CO_3)_2$ and $Ca(NO_3)_2{\cdot}4H_2O$ being detected for the first time in Greenland ice. We also found many particles with strong bands between 100 and 600 cm^{-1}, as shown in Figure 6e, which are similar to the spectra for silica minerals [*Kihara et al.*, 2005]. However, not all silica minerals were identified. Among 423 particles, 39 of $CaSO_4{\cdot}2H_2O$, 21 of $CaCO_3$, 5 of $Ca(NO_3)_2{\cdot}4H_2O$, 2 of $CaMg(CO_3)_2$, and 147 of silica minerals were detected (Figure 7a). The number ratio of $CaSO_4{\cdot}2H_2O$ to that of the sum of $CaCO_3$, $Ca(NO_3)_2{\cdot}4H_2O$, and $CaMg(CO_3)_2$ is 1.39 ± 0.35. Thus, $CaSO_4$ exists about 1.4 more often as the sum of $CaCO_3$, $Ca(NO_3)_2{\cdot}4H_2O$, and $CaMg(CO_3)_2$.

The same samples were also analyzed by SEM-EDS. We made a classification of the nonvolatile particles based on their elemental composition. Particles containing Ca and S are regarded as $CaSO_4$. Those with Ca, no S, and no Cl are classified as CaX. Those with Na and Cl are NaCl. Those with Na and S are Na_2SO_4. Those with S, no Ca, and no Na are classified as S-nCaNa. Those with Cl, no Ca, and no Na are Cl-nCaNa. Finally, those without any Si, S, Cl, Ca, and Na are classified as Other. The Si-containing particles are classified as insoluble particles. In total, 414 particles were measured: 45 of $CaSO_4$, 51 of CaX, 62 of NaCl, 18 of Na_2SO_4, 1 of NaX, 1 of S-nCaNa, 13 of Cl-nCaNa, 11 of Other, and 382 insoluble particles were detected (Figure 7b). The number ratio of $CaSO_4$ to the CaX is 0.88 ± 0.33. This ratio agrees with that of the micro-Raman measurement within mutual error. Thus, CaX can be considered as $CaCO_3$, $Ca(NO_3)_2$, or $CaMg(CO_3)_2$. As Figure 7a shows, $CaCO_3$ is the dominant component in these three salts; CaX can be regarded as $CaCO_3$.

3.4. Number Fractions of the Particle Compositions Over the Last 110 kyr

We now consider how the particle compositions vary through the six climatic stages (see section 2.1). In the last glacial period, the average number ratio of insoluble dust to nonvolatile aerosols (Si particle/total) is higher than that in the Holocene (Figure 8b). In particular, the ratio is higher in the colder stages of LGM and GS than that in milder stages of YD and GI. This indicates that the contribution of silicate particles (terrestrial dust) to total nonvolatile aerosols is higher in colder climate stages.

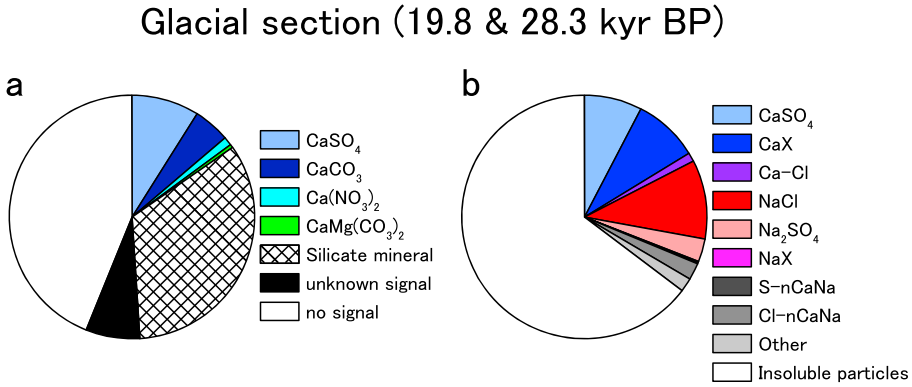

Figure 7. Number fraction of particles of glacial sections measured by the micro-Raman spectrometer and the SEM-EDS. (a) Number fraction of particles analyzed by the micro-Raman spectrometer. The particles showing bands between 100 and 600 cm^{-1} are classified as "silicate minerals." Particles showing spectra that could not be identified are indicated as "unknown signal." Particles showing no spectral features are classified as "no Raman signal." (b) Number fraction of particles analyzed by SEM-EDS. See the main text for the classification.

According to section 3.2, Ca-containing particles (Ca salts) are a proxy of soluble terrestrial material. The ratio of Ca salts to total particles is higher in the cold stages of YD, LGM, GI, and GS than in the warmer Holocene and BA stages (Figure 8c). Focusing on just the last glacial period, Ca salts/total in the milder YD and GI stages are higher than those in the colder LGM and GS stages, which is the opposite trend as Si particle/total. The production rate of Ca salts such as $CaCO_3$ is controlled by the wet-dry cycle in the source region [*Liu and Ding*, 1998]. Thus, consistent with *Ruth et al.* [2007], we find that although both the Ca salts and insoluble dust are a proxy for terrestrial material, our results also imply that the behavior of calcium compounds differ from

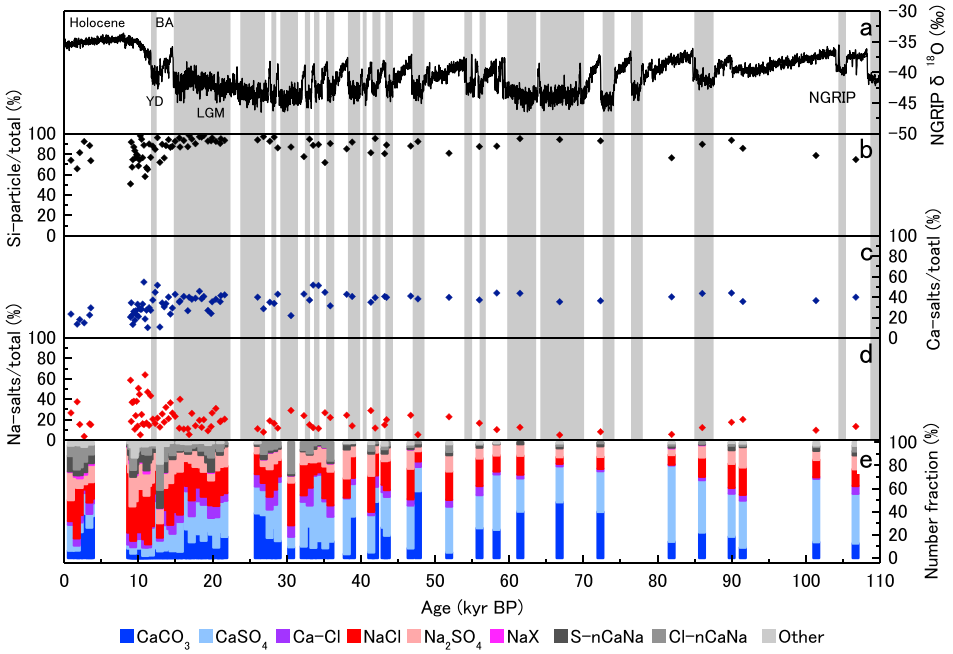

Figure 8. Time series of the number ratio of silicate dust and soluble salts in relation to all nonvolatile particles for the last 110 kyr B.P. (a) NGRIP $\delta^{18}O$ profile on GICC05 (younger than 60.2 ka before A.D. 2000) and GICC05modelext (older than 60.2 ka before A.D. 2000) [*Rasmussen et al.*, 2014, and their references]. (b) Si-containing particle (silicate dust) in relation to total nonvolatile particles. (c) Ca salts particle in relation to total nonvolatile particles. (d) Na salts particle in relation to total nonvolatile particles. (e) Time series of number fraction of soluble components. Color legends are the same as those in Figure 5. Gray shading indicates Younger Dryas, LGM, and glacial stadials.

Table 3. Salt Fractions and Concentrations

	Number Fraction									Mass Fraction						Concentration (μmol/L)			
Age (kyr B.P.)	$CaCO_3$	$CaSO_4$	Ca-Cl	NaCl	Na_2SO_4	NaX	S-nCaNa	Cl-nCaNa	Other	$CaCO_3$	$CaSO_4$	Ca-Cl	NaCl	Na_2SO_4	NaX	$CaCO_3$	$CaSO_4$	NaCl	Na_2SO_4
0.9	0.064	0.224	0.032	0.181	0.243	0.006	0.132	0.090	0.028	0.223	0.195	0.013	0.133	0.067	0.369				
1.7	0.065	0.044	0.062	0.439	0.093	0.014	0.049	0.213	0.021	0.023	0.244	0.014	0.583	0.068	0.067				
2.1	0.225	0.084	0.064	0.235	0.084	0.027	0.067	0.191	0.023	0.006	0.675	0.015	0.238	0.014	0.052				
2.7	0.383	0.180	0.030	0.045	0.083	0.023	0.090	0.128	0.038	0.055	0.823	0.012	0.054	0.035	0.021				
3.4	0.263	0.119	0.099	0.259	0.123	0.012	0.041	0.070	0.012	0.025	0.592	0.028	0.123	0.035	0.199				
3.6	0.363	0.111	0.040	0.143	0.148	0.017	0.074	0.086	0.017	0.083	0.711	0.028	0.089	0.037	0.051				
8.9	0.082	0.035	0.104	0.590	0.148	0.006	0.016	0.016	0.003	0.017	0.152	0.018	0.609	0.085	0.119	0.26	0.03	0.29	0.04
9.0	0.187	0.249	0.093	0.213	0.151	0.000	0.053	0.049	0.004	0.122	0.657	0.059	0.118	0.040	0.004	0.13	0.02	0.28	0.09
9.2	0.083	0.212	0.008	0.145	0.369	0.033	0.091	0.017	0.041	0.063	0.355	0.001	0.089	0.227	0.264	0.18	0.03	0.07	0.17
9.3	0.038	0.056	0.056	0.397	0.157	0.000	0.059	0.220	0.017	0.025	0.182	0.017	0.626	0.076	0.073	0.11	0.02	0.34	0.04
9.4	0.120	0.065	0.117	0.396	0.140	0.000	0.026	0.130	0.006	0.016	0.305	0.045	0.413	0.211	0.011	0.14	0.01	0.28	0.14
9.5	0.234	0.202	0.000	0.056	0.226	0.016	0.137	0.000	0.129	0.401	0.343	0.000	0.034	0.185	0.037	0.10	0.12	0.04	0.24
9.6	0.130	0.223	0.021	0.239	0.197	0.000	0.076	0.029	0.084	0.145	0.319	0.005	0.122	0.325	0.083	0.15	0.07	0.12	0.33
9.8	0.131	0.103	0.050	0.411	0.188	0.004	0.043	0.050	0.021	0.123	0.161	0.014	0.443	0.143	0.116	0.12	0.09	0.34	0.11
9.9	0.185	0.399	0.006	0.121	0.162	0.012	0.052	0.029	0.035	0.214	0.170	0.007	0.419	0.078	0.112	0.11	0.13	0.32	0.06
10.0	0.083	0.083	0.058	0.442	0.255	0.015	0.031	0.018	0.015	0.020	0.336	0.015	0.391	0.128	0.110	0.19	0.01	0.33	0.11
10.2	0.108	0.136	0.063	0.364	0.264	0.014	0.020	0.017	0.014	0.073	0.232	0.037	0.374	0.206	0.078	0.16	0.05	0.25	0.14
10.3	0.476	0.270	0.000	0.032	0.127	0.000	0.087	0.000	0.008	0.082	0.898	0.000	0.007	0.013	0.000	0.26	0.02	0.17	0.31
10.4	0.174	0.184	0.068	0.174	0.261	0.005	0.087	0.048	0.000	0.066	0.236	0.016	0.419	0.212	0.051	0.21	0.06	0.27	0.14
10.6	0.184	0.328	0.035	0.129	0.149	0.010	0.144	0.010	0.010	0.144	0.118	0.004	0.303	0.186	0.245	0.09	0.11	0.18	0.11
10.8	0.106	0.204	0.389	0.181	0.079	0.000	0.011	0.011	0.019	0.116	0.546	0.224	0.090	0.020	0.004	0.19	0.04	0.36	0.08
10.9	0.019	0.072	0.072	0.523	0.189	0.002	0.024	0.065	0.034	0.042	0.115	0.058	0.583	0.114	0.088	0.19	0.07	0.36	0.07
11.1	0.094	0.356	0.010	0.079	0.194	0.026	0.199	0.026	0.016	0.321	0.139	0.004	0.143	0.244	0.149	0.09	0.21	0.14	0.24
11.3	0.040	0.054	0.025	0.505	0.202	0.000	0.069	0.079	0.025	0.019	0.108	0.013	0.606	0.143	0.111	0.20	0.04	0.33	0.08
11.5	0.164	0.386	0.018	0.088	0.199	0.000	0.123	0.006	0.018	0.309	0.530	0.016	0.061	0.068	0.016	0.34	0.20	0.28	0.32
11.7	0.022	0.241	0.014	0.377	0.291	0.000	0.030	0.017	0.008	0.210	0.058	0.021	0.442	0.161	0.107	0.09	0.31	0.33	0.12
12.0	0.163	0.330	0.066	0.273	0.119	0.000	0.004	0.035	0.009	0.407	0.323	0.032	0.203	0.021	0.014	1.01	1.28	1.70	0.18
12.3	0.162	0.421	0.035	0.147	0.154	0.000	0.050	0.008	0.023	0.390	0.382	0.103	0.103	0.023	0.000	1.15	1.17	1.42	0.31
12.6	0.085	0.442	0.078	0.169	0.169	0.000	0.016	0.022	0.019	0.361	0.541	0.006	0.063	0.027	0.001	2.58	1.72	1.68	0.72
12.9	0.059	0.091	0.027	0.124	0.129	0.005	0.156	0.226	0.183	0.196	0.298	0.016	0.133	0.231	0.126	0.44	0.29	0.21	0.37
13.2	0.179	0.121	0.146	0.307	0.107	0.004	0.014	0.107	0.014	0.044	0.201	0.070	0.568	0.070	0.046	0.79	0.17	0.97	0.12
13.5	0.066	0.310	0.041	0.190	0.132	0.004	0.095	0.145	0.017	0.454	0.267	0.039	0.105	0.093	0.042	0.35	0.59	0.35	0.31
13.7	0.079	0.207	0.131	0.341	0.134	0.007	0.020	0.052	0.030	0.103	0.456	0.110	0.297	0.018	0.016	0.51	0.11	0.64	0.04
14.1	0.083	0.424	0.003	0.141	0.241	0.000	0.066	0.041	0.000	0.568	0.265	0.022	0.042	0.097	0.006	0.49	1.04	0.44	1.01
14.3	0.086	0.165	0.037	0.362	0.226	0.000	0.074	0.045	0.004	0.091	0.165	0.018	0.445	0.232	0.048	0.44	0.24	0.55	0.29
14.6	0.060	0.150	0.188	0.335	0.124	0.000	0.034	0.109	0.000	0.052	0.238	0.072	0.561	0.042	0.035	0.39	0.09	0.58	0.04
15.0	0.126	0.317	0.099	0.229	0.167	0.003	0.038	0.020	0.000	0.347	0.447	0.049	0.066	0.039	0.052	2.19	1.70	1.09	0.65
15.5	0.220	0.298	0.119	0.167	0.119	0.000	0.018	0.054	0.006	0.163	0.626	0.065	0.092	0.054	0.001	2.50	0.65	1.51	0.88
15.6	0.055	0.259	0.063	0.371	0.176	0.000	0.012	0.063	0.002	0.404	0.312	0.029	0.219	0.026	0.011	1.38	1.78	1.88	0.22
16.1	0.335	0.266	0.106	0.133	0.090	0.000	0.027	0.032	0.011	0.128	0.766	0.037	0.046	0.022	0.000	4.84	0.81	2.05	0.97
16.7	0.248	0.331	0.045	0.218	0.060	0.000	0.023	0.060	0.015	0.060	0.117	0.021	0.653	0.046	0.102	3.50	1.79	2.24	0.16
16.8	0.542	0.253	0.047	0.058	0.068	0.000	0.024	0.008	0.000	0.120	0.848	0.016	0.011	0.004	0.000	6.11	0.87	2.48	0.95
17.2	0.137	0.226	0.137	0.326	0.119	0.000	0.011	0.044	0.000	0.157	0.475	0.089	0.236	0.038	0.005	4.31	1.43	2.73	0.44
17.7	0.220	0.379	0.042	0.150	0.145	0.000	0.033	0.028	0.005	0.414	0.481	0.012	0.069	0.019	0.005	2.70	2.32	2.81	0.75
18.2	0.207	0.285	0.119	0.219	0.126	0.004	0.019	0.022	0.000	0.213	0.580	0.077	0.097	0.032	0.001	4.04	1.48	4.20	1.40
18.5	0.255	0.281	0.108	0.143	0.106	0.000	0.039	0.067	0.002	0.237	0.581	0.052	0.092	0.034	0.005	3.37	1.37	2.36	0.88
18.8	0.149	0.313	0.069	0.215	0.174	0.000	0.028	0.052	0.000	0.215	0.428	0.096	0.174	0.087	0.000	2.92	1.47	2.06	1.04
19.4	0.276	0.262	0.041	0.193	0.055	0.000	0.069	0.083	0.021	0.131	0.447	0.012	0.349	0.014	0.047	3.57	1.05	2.67	0.11

Journal of Geophysical Research: Atmospheres

10.1002/2015JD023290

Journal of Geophysical Research: Atmospheres

10.1002/2015JD023290

Table 3. (continued)

	Number Fraction									Mass Fraction						Concentration (μmol/L)			
Age (kyr B.P.)	$CaCO_3$	$CaSO_4$	Ca-Cl	NaCl	Na_2SO_4	NaX	S-nCaNa	Cl-nCaNa	Other	$CaCO_3$	$CaSO_4$	Ca-Cl	NaCl	Na_2SO_4	NaX	$CaCO_3$	$CaSO_4$	NaCl	Na_2SO_4
19.8	0.231	0.117	0.110	0.214	0.065	0.010	0.123	0.123	0.006	0.063	0.526	0.101	0.272	0.034	0.005	3.58	0.43	3.35	0.42
19.9	0.203	0.211	0.070	0.344	0.145	0.000	0.008	0.020	0.000	0.196	0.576	0.007	0.208	0.012	0.001	4.04	1.37	2.46	0.14
20.5	0.091	0.263	0.097	0.308	0.166	0.000	0.026	0.049	0.000	0.204	0.328	0.051	0.319	0.075	0.023	3.36	2.10	2.68	0.63
21.0	0.243	0.243	0.060	0.243	0.106	0.000	0.032	0.069	0.005	0.247	0.592	0.018	0.093	0.044	0.006	5.18	2.16	2.57	1.21
21.1	0.225	0.276	0.100	0.237	0.110	0.000	0.014	0.036	0.002	0.205	0.655	0.054	0.070	0.016	0.001	5.19	1.62	3.21	0.75
21.6	0.184	0.313	0.066	0.232	0.173	0.000	0.022	0.011	0.000	0.344	0.503	0.036	0.080	0.038	0.000	3.95	2.71	2.67	1.26
26.1	0.387	0.233	0.107	0.179	0.065	0.000	0.016	0.009	0.004	0.099	0.854	0.016	0.027	0.004	0.000	6.23	0.72	3.10	0.49
26.9	0.372	0.217	0.062	0.146	0.056	0.003	0.045	0.099	0.000	0.157	0.783	0.024	0.032	0.003	0.001	6.67	1.33	3.25	0.34
27.7	0.175	0.245	0.112	0.238	0.143	0.002	0.024	0.061	0.000	0.161	0.660	0.050	0.082	0.039	0.008				
28.3	0.260	0.202	0.131	0.228	0.103	0.004	0.020	0.052	0.000	0.121	0.761	0.043	0.057	0.018	0.000				
28.8	0.146	0.513	0.048	0.144	0.096	0.000	0.017	0.037	0.000	0.507	0.463	0.009	0.016	0.005	0.001				
30.6	0.093	0.091	0.100	0.369	0.060	0.002	0.020	0.264	0.000	0.062	0.334	0.149	0.373	0.060	0.022				
32.3	0.100	0.387	0.057	0.270	0.111	0.000	0.011	0.065	0.000	0.265	0.437	0.017	0.227	0.043	0.011				
33.1	0.273	0.182	0.154	0.222	0.063	0.000	0.012	0.093	0.000	0.051	0.914	0.011	0.017	0.006	0.001				
33.6	0.089	0.624	0.012	0.106	0.115	0.000	0.031	0.024	0.000	0.545	0.393	0.035	0.015	0.012	0.000				
34.3	0.147	0.575	0.021	0.093	0.138	0.002	0.012	0.012	0.000	0.589	0.391	0.006	0.004	0.009	0.002				
35.2	0.085	0.406	0.027	0.275	0.162	0.004	0.004	0.037	0.000	0.322	0.402	0.032	0.176	0.050	0.017				
35.9	0.142	0.216	0.099	0.292	0.071	0.003	0.020	0.157	0.000	0.227	0.664	0.020	0.070	0.013	0.006				
38.1	0.033	0.483	0.007	0.167	0.250	0.000	0.047	0.010	0.003	0.625	0.179	0.020	0.093	0.076	0.006				
38.8	0.360	0.281	0.054	0.187	0.094	0.000	0.020	0.000	0.005	0.195	0.551	0.014	0.218	0.008	0.014				
41.4	0.048	0.324	0.029	0.311	0.192	0.000	0.026	0.058	0.013	0.277	0.336	0.037	0.265	0.075	0.010				
41.9	0.486	0.131	0.098	0.197	0.066	0.000	0.016	0.005	0.000	0.081	0.830	0.019	0.059	0.010	0.001				
43.2	0.263	0.308	0.064	0.205	0.064	0.000	0.038	0.032	0.026	0.068	0.838	0.006	0.075	0.006	0.008				
43.5	0.193	0.336	0.059	0.256	0.113	0.000	0.017	0.025	0.000	0.202	0.608	0.013	0.154	0.016	0.008				
46.7	0.084	0.371	0.054	0.264	0.167	0.003	0.020	0.020	0.017	0.244	0.389	0.044	0.246	0.039	0.038				
47.7	0.578	0.211	0.048	0.088	0.041	0.000	0.027	0.007	0.000	0.145	0.791	0.010	0.033	0.003	0.017				
51.9	0.048	0.397	0.059	0.246	0.140	0.000	0.029	0.066	0.015	0.354	0.162	0.041	0.328	0.071	0.044				
56.0	0.257	0.287	0.079	0.238	0.094	0.000	0.025	0.010	0.010	0.308	0.537	0.015	0.128	0.010	0.003				
58.3	0.245	0.480	0.026	0.138	0.097	0.000	0.005	0.005	0.005	0.484	0.433	0.010	0.058	0.015	0.000				
61.5	0.402	0.287	0.033	0.163	0.100	0.000	0.014	0.000	0.000	0.121	0.804	0.007	0.056	0.011	0.000				
66.8	0.482	0.312	0.021	0.057	0.078	0.000	0.021	0.021	0.007	0.181	0.801	0.002	0.011	0.005	0.000				
72.3	0.399	0.353	0.020	0.105	0.092	0.000	0.026	0.007	0.000	0.155	0.782	0.003	0.046	0.013	0.002				
81.9	0.141	0.660	0.006	0.083	0.058	0.006	0.019	0.019	0.006	0.550	0.382	0.016	0.031	0.013	0.008				
86.0	0.220	0.455	0.029	0.167	0.105	0.005	0.010	0.010	0.000	0.358	0.487	0.017	0.085	0.048	0.005				
90.0	0.184	0.373	0.051	0.208	0.118	0.000	0.039	0.024	0.004	0.190	0.559	0.029	0.193	0.020	0.010				
91.5	0.090	0.408	0.049	0.238	0.175	0.000	0.013	0.018	0.009	0.367	0.378	0.031	0.130	0.059	0.035				
101.4	0.137	0.549	0.013	0.150	0.078	0.000	0.033	0.013	0.026	0.296	0.208	0.003	0.441	0.043	0.009				
106.7	0.126	0.430	0.068	0.145	0.121	0.000	0.034	0.048	0.029	0.436	0.319	0.054	0.120	0.054	0.016				

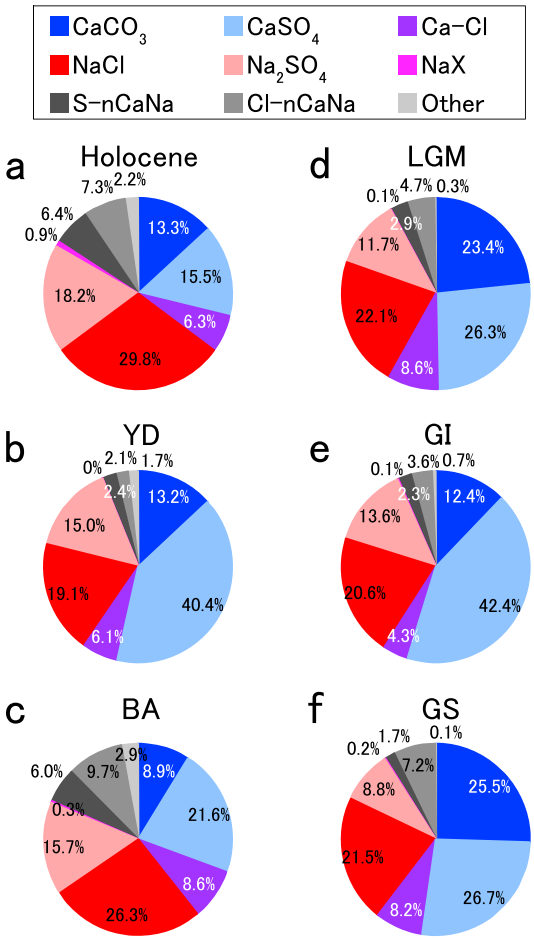

Figure 9. Number fractions of soluble components in each of the six climatic stages. Color legends are the same as those in Figure 5.

silicate dust. The Na salts are particles containing Na but not Si. They are soluble salt particles and a proxy of sea salt. The ratio of Na salts/total is higher in warmer stages than in colder stages (Figure 8d).

The number fraction of Ca salts is higher than that of Na salts in the last glacial period and vice versa in the Holocene (Figure 8e and Table 3). In the YD, LGM, GI, and GS, Ca salts accounts for more than half of the total soluble particles. Among these cold stages, the number fraction of $CaSO_4$ accounts for much more than half of the total Ca salts in YD and GI (Figures 9b and 9e). On the other hand, the fraction of $CaSO_4$ is almost the same as that of $CaCO_3$ in LGM and GS (Figures 9d and 9f). In the Holocene, the Na salts account for half of the total soluble particles (Figure 9a and Table 3). And among the Na salts, nearly all are NaCl and Na_2SO_4. The NaCl and Na_2SO_4 are the most common Na salts in all six climatic stages (Figure 9). Also, in the Holocene, the fractions of sulfate salt particles without Na, Ca, Mg, and K are larger than those of all particles (e.g., Figures 4d, 4e, 10a, and 10b). This sulfate salt can be assumed to be $(NH_4)_2SO_4$ one of the most common sulfate salts at present [*Willison et al.*, 1989]. In contrast to the Holocene, YD, LGM, GI, and GS, the BA record has a nearly equal fraction of both Ca salts to Na salts (Figure 9c).

In this way, six climatic stages can be sorted into three groups depending on the fractions of Ca and Na salts; the Glacial group (YD, LGM, GI, and GS), the Holocene, and BA. The Ca salts account for more than half of the total soluble particles in the Glacial group; it accounts for about half of the total soluble particles in the Holocene, and the fractions of Ca and Na salts are nearly equal in the BA. This indicates that the contribution of terrestrial material was higher than that of sea salt in the Glacial group, the contribution of sea salt was higher than that of terrestrial material in the Holocene, and the BA may be a transition period in which the terrestrial and sea-salt contributions to soluble salts were roughly equal. Moreover, the Glacial group can be divided further into two types in terms of their $CaCO_3$ and $CaSO_4$ fractions: the cold type (LGM and GS) and the mild type (YD and GI).

3.5. Mole Fractions and Concentrations of Ca Salts and Na Salts

We discuss the difference in the major soluble salts of $CaCO_3$, $CaSO_4$, NaCl, and Na_2SO_4 in each climatic stage by comparison with ion concentrations. For this purpose, we need to use the ion concentrations, but available data for the NEEM ice core are limited. Instead, we use those from GRIP, which should provide a representative record for the Greenland ice sheet [*De Angelis et al.*, 1997; *Fuhrer and Legrand*, 1997; *Legrand et al.*, 1997] (Table 4).

Number ratios of Ca salts and Na salts were converted into mass ratios (Figure 12). Ca salts include $CaCO_3$, $CaSO_4$, and Ca-Cl particles, and the Na salts include NaCl, Na_2SO_4, and soluble Na particles other than NaCl and Na_2SO_4 (NaX). The Ca salts are soluble Ca, and the Na salts are soluble Na, which are equivalent to Ca^{2+}

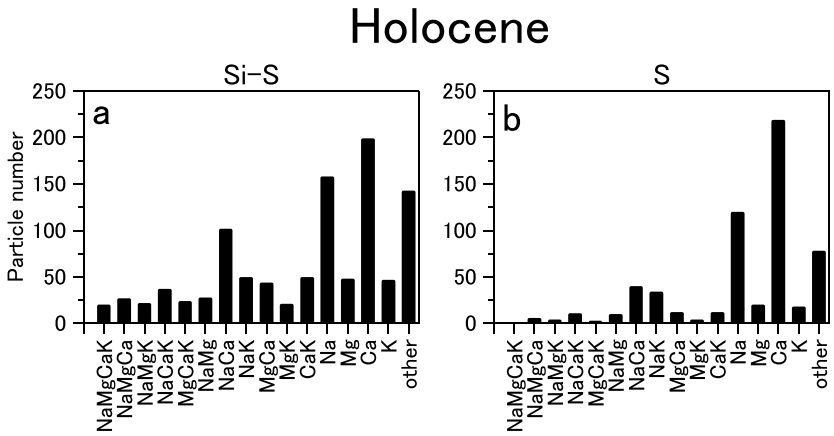

Figure 10. Same as Figure 4 except for the Si-S particles and S particles of the Holocene sample.

and Na^+, respectively. This assumption should be safe because soluble Na/Ca of the sublimation method corresponds to Na^+/Ca^{2+} of the NEEM ice core within the margin of error (Figure 11).

Here we compare sublimation results with the GRIP ion concentrations. Mass ratios are basically consistent with the number ratios discussed in section 3.4 (Figure 12a), indicating that the major salts are $CaCO_3$, $CaSO_4$, NaCl, and Na_2SO_4. Also, Holocene ice has higher Na salt mass ratios, whereas glacial ice has higher Ca salt mass ratios. These are consistent with the GRIP cation concentrations in which the Na^+ concentration exceeds that of Ca^{2+} in the Holocene and Ca^{2+} is the dominant cation in the Glacial group (Table 4).

For the Ca salts, $CaCO_3$ is the dominant component of Ca^{2+} over the last 110 kyr because mass ratio of $CaCO_3/CaSO_4$ lies above 1 (i.e., $CaCO_3 > CaSO_4$) more than 75% of the entire period. During the last glacial period, $CaCO_3/CaSO_4$ is higher in the LGM and GS (cold type) than in the YD and GI (mild type) (Figure 12b), which means that the ratio of $CaSO_4$ to Ca^{2+} is higher in the warmer climate stages during a glacial period. About 45% of the Ca^{2+} is present as $CaSO_4$ in the mild-type stages (45.9 and 43.5% in YD and GI), whereas about 25% of Ca^{2+} is present as $CaSO_4$ in cold-type stages (26.4 and 21.3% in LGM and GS). On the other hand, the Holocene has a high $CaCO_3/CaSO_4$ ratio (Figure 12b). In this case, the $CaCO_3$ ratio may have actually been high or perhaps instead the $Ca(NO_3)_2$ ratio was high (SEM-EDS does not distinguish between $CaCO_3$ and $Ca(NO_3)_2$). Since NO_3^- is the dominant anion in the Holocene (Table 4), nitrate salts may have been present in the Holocene ice.

Higher ratio of $CaSO_4$ in YD and GI than in LGM and GS indicates that the sulfatization of $CaCO_3$ in YD and GI was more intense compared to LGM and GS. Possible explanations are that (i) transport was faster in the cold-type stages, giving less time for reaction or (ii) not enough sulfate was present to react with $CaCO_3$ in the atmosphere as previous studies discussed [e.g., *De Angelis et al.*, 1997; *Legrand et al.*, 1997; *Ruth and Wagenbach*, 2003; *Fischer et al.*, 2007; *Iizuka et al.*, 2008]. Also, the production rate of evaporites including gypsum varied between wet and dry climatic phases [*Xingqi et al.*, 2008], so another possible explanation is that (iii) the emission rate of gypsum differed between cold-type stages and mild-type stages.

Table 4. Ion Concentrations of GRIP Samples (μmol/L) [*De Angelis et al.*, 1997; *Fuhrer and Legrand*, 1997; *Legrand et al.*, 1997]

Climate Stage	Group	Type	Ca^{2+}	Na^+	NH_4^+	SO_4^{2-}	Cl^-	NO_3^-	Cl^-/Na^{+a}
Holocene (0.9–11.7 kyr B.P.)	Holocene	Warm	0.20 ± 0.13	0.25 ± 0.14	0.46 ± 0.37	0.49 ± 0.28	0.42 ± 0.19	1.22 ± 0.23	1.87
YD (12.0–12.6 kyr B.P.)	Glacial	Mild	2.35 ± 1.07	1.44 ± 0.65	1.32 ± 1.20	1.10 ± 0.23	1.91 ± 0.71	1.67 ± 0.45	1.71
BA (12.9–14.6 kyr B.P.)	BA	Warm	0.92 ± 0.28	0.82 ± 0.27	0.57 ± 0.32	0.81 ± 0.23	1.14 ± 0.26	1.30 ± 0.23	1.62
LGM (15.0–26.9 kyr B.P.)	Glacial	Cold	6.80 ± 1.75	2.25 ± 0.71	0.17 ± 0.09	2.54 ± 0.55	2.79 ± 0.25	1.26 ± 0.25	1.47
GI (27.7–106.7 kyr B.P.)	Glacial	Mild	0.96 ± 0.22	0.69 ± 0.12	0.39 ± 0.21	0.55 ± 0.20	0.87 ± 0.13	1.02 ± 0.11	1.79
GS (28.3–86.0 kyr B.P.)	Glacial	Cold	5.69 ± 2.07	1.99 ± 0.97	0.34 ± 0.09	2.02 ± 1.62	2.02 ± 0.73	1.19 ± 0.15	1.47

[a] Cl^-/Na^+ of the bulk seawater is 1.8 [*Whitlow et al.*, 1992].

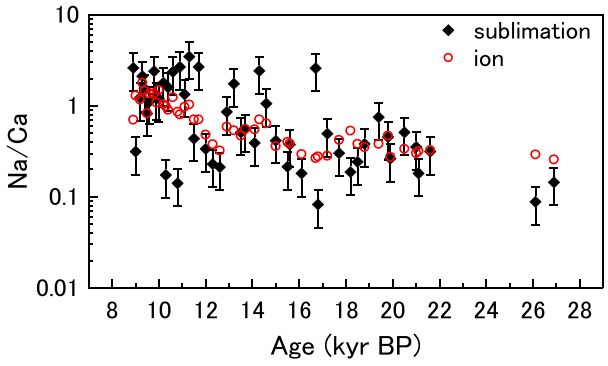

Figure 11. Soluble Na/Ca derived from the sublimation method and that from the NEEM ion concentration.

Given the much stronger glacial/interglacial and stadial/interstadial decrease of Ca^{2+} compared to SO_4^{2-}, option (ii) appears straight forward to explain our observations; however, our interpretation in terms of sulfatization in the atmosphere hinges on this open question.

For Na salt, NaCl is the dominant component of Na^+ over the last 110 kyr, with the mass ratio of $NaCl/Na_2SO_4$ exceeding 1 (i.e., $NaCl > Na_2SO_4$) more than 90% of the entire period. The $NaCl/Na_2SO_4$ ratio is higher in the YD, LGM, GI, and GS than in BA and early Holocene (Figure 12c). More than 70% of Na^+ is present as NaCl in YD, LGM, GI, and GS (78.7, 75.7, 71.2, and 75.4% in YD, LGM, GI and GS, respectively), whereas 60.3 and 54.5% of Na^+ is present as NaCl in the BA and Holocene, respectively. This result indicates that Na^+ sulfatization may have occurred efficiently in warmer climate stages, because more sulfate was available to form Na_2SO_4 due to reduction of Ca^{2+} [*Röthlisberger et al.*, 2003]. In fact, the SO_4^{2-} concentration (eq) is higher than the sum of the Ca^{2+} and Na^+ concentrations (e.q.) in the Holocene (Table 4).

We compared the ratio of $NaCl/Na_2SO_4$ with the ratio of Cl^-/Na^+ of the GRIP ice core. If the Cl^-/Na^+ ratio in snow and ice was close to the ratio of seawater, Na^+ have been considered to be present as NaCl in previous studies [e.g., *De Angelis et al.*, 1997; *Röthlisberger et al.*, 2003]. The Cl^-/Na^+ was relatively high and scattered during the Holocene, with slightly higher values at the beginning of the Holocene [*De Angelis et al.*, 1997], but the average value is close to the bulk seawater value from the last glacial period to Holocene (Table 4). Based only on this ion ratio, most of the Na^+ would be assumed to be present as NaCl. However, not all Na^+ was present as NaCl as Figure 12a shows. In particular, the Na_2SO_4 ratio is high in the Holocene. Therefore, salt composition cannot be simply derived from the ion ratio only.

$CaCO_3$, $CaSO_4$, NaCl, and Na_2SO_4 concentrations are calculated by focusing on the deglaciation, the largest climatic transition in the last 110 kyr. These concentrations are obtained by multiplying Ca^{2+} or Na^+ of the

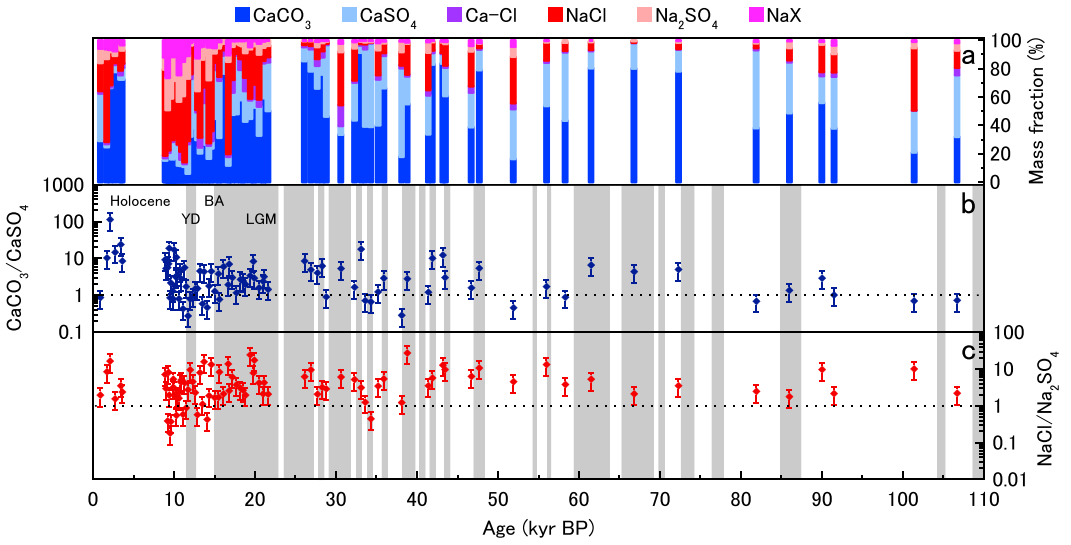

Figure 12. Mole fraction and ratios over the last 110 kyr. (a) Mole fraction of Ca salts and Na salts. Color legends are the same as those in Figure 5. (b) Mass ratio of $CaCO_3$ to $CaSO_4$. (c) Mass ratio of NaCl to Na_2SO_4. Gray shading indicates Younger Dryas, LGM, and glacial stadials.

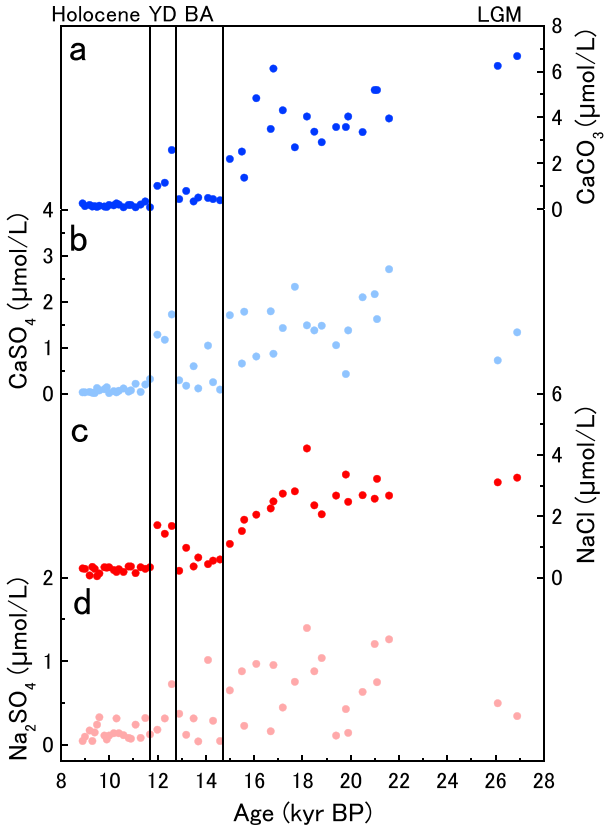

Figure 13. Salts concentrations over the deglaciation. (a) $CaCO_3$ concentration. (b) $CaSO_4$ concentration. (c) NaCl concentration. (d) Na_2SO_4 concentration.

NEEM ice core by the mass ratio of Ca salt or Na salt shown in Figure 12a. For example, the $CaCO_3$ concentration is obtained by multiplying the Ca^{2+} concentration by the mass ratio of $CaCO_3$ to soluble Ca ($CaCO_3$ $CaSO_4$ + Ca-Cl). Results are shown in Figures 13a–13d and Table 3. Between climate stages, Ca salt concentrations change more than Na salt, with the Na_2SO_4 having the least change of all four salts. For example, compared to the Holocene values, the $CaCO_3$ concentrations in the LGM, BA, and YD are a factor of 25, 3, and 10 higher. If all of this $CaCO_3$ was converted to CO_2, it would have the potential to raise the CO_2 concentration measured in the gas phase by 4 ± 1 ppmv in the Holocene ice and 90 ± 30 ppmv in the LGM ice, respectively. These correspond to about 1% of the Holocene concentration (280 ppmv) and 50% of the LGM concentration (180 ppmv) [*Petit et al.*, 1999]. In comparison, the $CaSO_4$ concentrations are a factor of 18, 5, and 17 higher in the LGM, BA, and YD than in the Holocene. The corresponding factors for NaCl are 10, 2, and 6, whereas those for Na_2SO_4 are 5, 2, and 3. In all climate stages, the absolute $CaCO_3$ concentration exceeds that of $CaSO_4$ and that of NaCl exceeds Na_2SO_4. However, as we described above, ratio of sulfate salts is higher in warmer climate stages than in colder climate stages (i.e., ratio of $CaSO_4$ to Ca^{2+} is higher in the YD than in the LGM, and that of Na_2SO_4 to Na^+ is higher in the Holocene and BA than in the YD and LGM). Namely, the ratio in primary aerosols ($CaCO_3$ and NaCl) is higher in colder climate stages, whereas ratio in secondary aerosols ($CaSO_4$ and Na_2SO_4) is higher in warmer climate stages.

Compared to the Dome Fuji core from inland Antarctica, the NEEM ice core from Greenland shows a stronger preservation of the primary aerosols of $CaCO_3$ and NaCl. At Dome Fuji, NaCl/Na_2SO_4 ratio is around 2 in the LGM and below 1 in the Holocene [*Oyabu et al.*, 2014], whereas in NEEM, NaCl/Na_2SO_4 does rarely show values below 1 (Figure 12c). The Na^+ sulfatization was increased from glacial period to the Holocene, both at Dome Fuji and NEEM, but the Holocene in Greenland differs, having more Na^+ as primary salt (NaCl). Also, most of the Ca^{2+} exists in $CaSO_4$ at Dome Fuji [*Sakurai et al.*, 2009; *Oyabu et al.*, 2014], showing Ca^{2+} sulfatization was less at NEEM even when the SO_4^{2-} concentration (eq) is higher than the sum of Ca^{2+} and Na^+ concentration (eq) in Holocene. In the case of inland Antarctica, most of the Ca^{2+} and Na^+ forms sulfate, if the SO_4^{2-} concentration is higher than the sum of Na^+ and Ca^{2+} concentrations [*Oyabu et al.*, 2014]; however, this rule does not apply as well to Greenland. For glacial periods, a possible cause of the higher preservation of $CaCO_3$ and NaCl is that transport was faster, giving less time for reaction, or there was not enough SO_4^{2-} to react with $CaCO_3$ and NaCl in the atmosphere. For the Holocene, a possible cause is that SO_4^{2-} forms other sulfate salts. As we implied in section 3.4, $(NH_4)_2SO_4$ may be present in the Holocene ice. $(NH_4)_2SO_4$ arises from the neutralization of SO_4^{2-} by NH_4^+ [*Warneck*, 1999; *Fuhrer et al.*, 1996], and because NH_4^+ is a major cation in the Holocene in Greenland (Table 4), the $(NH_4)_2SO_4$ fraction should be relatively large in the Holocene.

3.6. Chemical Compositions of Nonvolatile Particles at Centimeter Resolution

In the following we will discuss the CFA records and chemical compositions of selected samples at centimeter resolution. For the LGM section, cloudy bands have high dust and ion concentrations, whereas clear layers

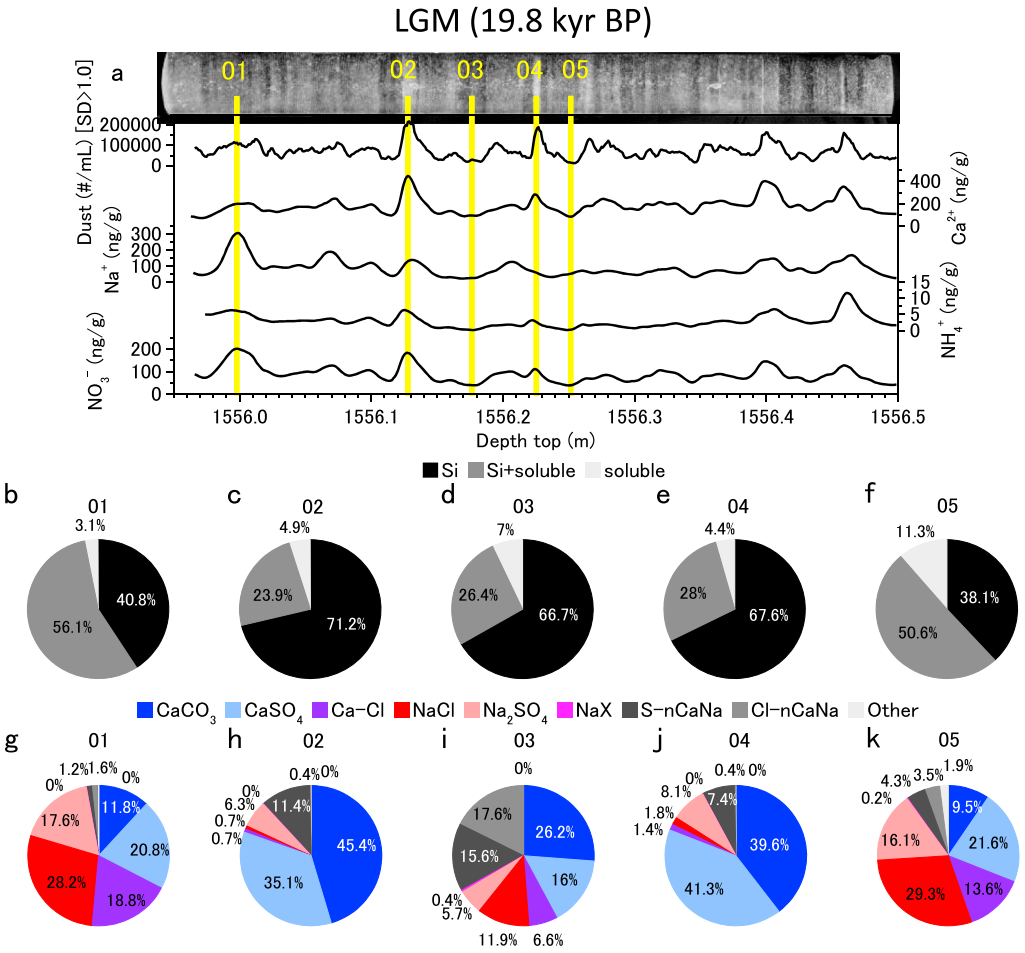

Figure 14. High-resolution analysis of the LGM section. (a) Dust, Ca^{2+}, Na^{+}, NH_4^{+}, and NO_3^{-} concentrations. (b to f) Number fraction of soluble and insoluble particles of subsamples 01–05. "Si" indicates particles containing Si but none of S and Cl (insoluble). "Si + soluble" indicates particles containing Si, S, and/or Cl. This particle is a mixture of insoluble dust and soluble salt particles. "Soluble" indicates particles without Si (soluble). (g to k) Number fraction of soluble salts of 01–05. See Figure 5 for color description.

have low dust and ion concentrations (Figure 14a). Thus, the dust concentrations clearly differ between cloudy bands and clear layers, yet more than 90% of the particles contain Si in all layers (Figures 14b–14f). This result shows that even in layers with a low dust concentration (clear layer), the fraction of mineral dust is high.

For the soluble components, Ca salts account for more than 80% of the soluble components in the cloudy bands (LGM-02 and LGM-04; Figures 14h and 14j). The Ca salts consist of $CaCO_3$ and $CaSO_4$ in the ratio 1:1. The fraction of Na salts is less than 10%, and most of it is in the form of Na_2SO_4. This result indicates also that the soluble components in the cloudy bands mainly consist of terrestrial materials. In contrast, the clear layers have a higher proportion (but still a low absolute concentration) of Na salts (LGM-01, LGM-03, and LGM-05; Figures 14g, 14i, and 14k). The Na salts consist of NaCl and Na_2SO_4, and more than 60% of the Na salt is in the form of NaCl. This result indicates that in clear layers, the relative contribution of sea salt to soluble components is higher than that in cloudy bands. The soluble components show clear differences between cloudy bands and clear layers even though both have more than 90% of their Si (dust) within nonvolatile particles.

For the Holocene section, ion and dust concentrations show clear seasonal variability, which makes it possible to determine seasonalities from their concentrations. Following previous studies [e.g., *Whitlow et al.*, 1992; *Fuhrer et al.*, 1996; *Legrand and Mayewski*, 1997; *Kuramoto et al.*, 2011; *Gfeller et al.*, 2014], the concentrations indicate that Holocene-01 is a winter layer (Na^{+} peak), Holocene-02 and Holocene-04 are summer layers (NH_4^{+} and NO_3^{-} peak), and Holocene-03 is a spring layer (dust and Ca^{2+} peak) (Figure 15a).

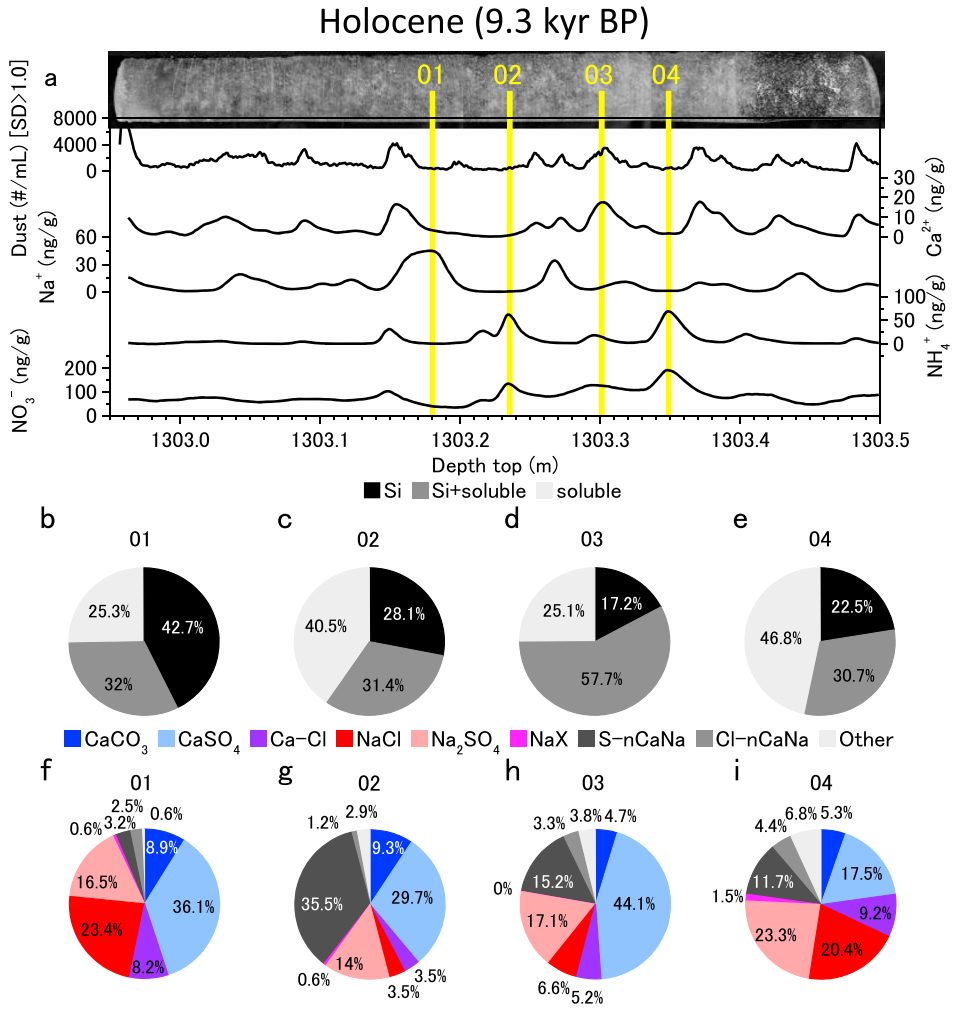

Figure 15. Same as Figure 14, except for the Holocene section.

The particle compositions in the Holocene also show clear seasonality. In Holocene-01 and Holocene-03 (winter and spring), 75% of the particles contain Si, whereas in Holocene-02 and Holocene-04 (summer), less than 60% of the particles contain Si (Figures 15b–15e). This suggests that the dust-to-nonvolatile ratio of particles in the winter and spring layers is higher than that of summer layer. Even in spring (dust season), the fraction of Si-containing particles is lower than that in the low-dust LGM clear layer. This result suggests that the atmosphere in the LGM has larger proportion of silicate minerals than that of the dust season in the Holocene.

Concerning the Holocene's soluble components, the fraction of Na salts in winter (Figure 15f) is larger than that of summer (Figure 15g) and spring (Figure 15h). Moreover, the fraction of NaCl is larger than that of Na_2SO_4, showing that the NaCl fraction is high in winter. A high Na salts fraction with high NaCl content suggests that the sulfatization of NaCl does not increase in winter. This trend in NaCl may be due to an increasing sea-salt (NaCl) emission and a decreasing DMS (SO_4^{2-}) emission. For the Ca salts, the fraction in spring (Figure 15h) exceeds that of winter (Figure 15f) and summer (Figure 15g), which indicates that the contribution of terrestrial material is high in spring layers. The $CaSO_4$ fraction is high in this layer. The high fraction suggests that much of the Ca^{2+}, which mainly originates from Asian deserts [e.g., *Svensson et al.*, 2000; *Bory et al.*, 2003], was sulfatized during its long-range transportation. Holocene-02 seems to represent summer aerosols (Figure 15g). In this sample, the fraction of "other salt" (S-nCaNa + Cl-nCaNa + Other) exceeds that of winter (Figure 15f) and spring (Figure 15h). Especially, the fraction of S-nCaNa is high. This S-nCaNa can be assumed to be $(NH_4)_2SO_4$ because both NH_4^+ and SO_4^{2-} peak in summer [*Kuramoto et al.*, 2011; *Gfeller et al.*, 2014] and thus likely react more at this time to form $(NH_4)_2SO_4$. In this way, salt compositions show clear seasonal variability in the Holocene ice section.

4. Conclusion

This study analyzed the chemical compositions of nonvolatile particles larger than 0.45 μm in Greenland over the last 110 kyr by using a sublimation method. We found that the dominant soluble compounds are $CaCO_3$, $CaSO_4$, NaCl, and Na_2SO_4 salts. In addition, $CaMg(CO_3)_2$ and $Ca(NO_3)_2{\cdot}4H_2O$ were detected for the first time in Greenland ice.

The occurrence of the major soluble compounds $CaCO_3$, $CaSO_4$, NaCl, and Na_2SO_4 is not the same during different climatic periods. In the Glacial group (YD, LGM, GI, and GS), the fraction of Ca salts ($CaCO_3 + CaSO_4$) exceeds that of Na salts ($NaCl + Na_2SO_4$), whereas the opposite is found in the Holocene. The Glacial group was subdivided into further two types: the cold type (LGM and GS) and the mild type (YD and GI). The $CaCO_3$ ratio is higher in the cold type than in the mild type, while for the $CaSO_4$ ratio the opposite is found. This result indicates that sulfatization of $CaCO_3$ was less frequent than that in the YD and GI due to the insufficient availability of SO_4^{2-} in the atmosphere in times of extraordinarily high Ca^{2+} abundance. In the Holocene, the fractions of not only NaCl but also Na_2SO_4 were higher than those in the Glacial group, indicating that more sulfatization of NaCl occurred in the Holocene. In the BA, the number ratio of Ca salts to Na salts is closer to 1 than that from the Holocene and the Glacial group. Mass fractions of Ca and Na salts were basically consistent with the number ratio: 45% of Ca^{2+} existed as $CaSO_4$ in mild-type stages, whereas 25% of Ca^{2+} existed as $CaSO_4$ in cold-type stages; more than 70% of Na^+ existed as NaCl in YD, LGM, GI, and GS, whereas 55–60% of Na^+ existed as NaCl in the Holocene and BA. In summary, sulfatization of primary aerosol in the atmosphere occurs on both sea salt and mineral dust aerosol with the most sulfatization taking place on the most abundant aerosol class. Note, however, that for the Holocene, ammonium sulfates have to be taken into account as well, which are formed by reaction of NH_3 with H_2SO_4.

By focusing on the last deglaciation, $CaCO_3$, $CaSO_4$, NaCl, and Na_2SO_4 were calculated. Ca salt concentrations changed more than Na salt concentration between different climate stages. Compared to the Holocene, the $CaCO_3$ and $CaSO_4$ concentrations were a factor of 3–5 higher in BA and 10–25 higher in YD and LGM. For NaCl, these factors were 2 and 6–10, whereas for Na_2SO_4 they were 2 and 3–5. The ratio of $CaSO_4$ to Ca^{2+} is higher in the YD than LGM, and that of Na_2SO_4 to Na^+ is higher in the Holocene and BA than in the YD and LGM, but for the absolute concentrations, $CaCO_3$ exceeds $CaSO_4$ and NaCl exceeds Na_2SO_4 in all stages.

Compared to the case in Dome Fuji in inland Antarctica, the NEEM ice core preserves more of the primary aerosols of $CaCO_3$ and NaCl. Possible explanations of preservation of $CaCO_3$ and NaCl for the glacial period are that transport was faster giving less time for reaction or not enough SO_4^{2-} was available to fully react with $CaCO_3$ and NaCl in the atmosphere. For the Holocene, one cause may be that SO_4^{2-} largely formed other sulfate salts such as $(NH_4)_2SO_4$.

High-resolution analyses were also done on the LGM and Holocene sections. For the LGM section, high-resolution analyses showed that more than 90% of the nonvolatile particles contain Si (dust). In the cloudy bands, Ca salts account for more than 80% of the soluble components, but clear layers account for more Na salts. For the Holocene section, the composition of soluble particles also shows clear seasonality. The winter layer contains more NaCl as compared to spring and summer layers. Conversely, the spring layer contains more Ca salts compared to summer and winter layers. Also, the $CaSO_4$ fraction is high in spring layer. The summer layer appears to contain more sulfate salt other than Na_2SO_4 and $CaSO_4$, and this salt may be $(NH_4)_2SO_4$.

Appendix A: Mole Calculation of Salts

The number of moles of the Ca and Na salts for each sample was calculated. The calculation procedure for the mole number is based on the previous study [*Oyabu et al.*, 2014], which was modified for this study. The number of moles of Na, Mg, Ca, K, S, and Cl are calculated by assuming that each particle is a sphere whose radius is calculated from its cross-sectional area on the SEM image. When a particle has Na and S, the equivalent of Na_2SO_4 is equal to the smaller equivalent of either Na or S. Here we express the equivalent of X, i.e., the number of ions in the solution caused by the species X, as [X]. If $[Na] < [S]$, then $[Na_2SO_4] = [Na]$. If $[Na] > [S]$, then $[Na_2SO_4] = [S]$. The same procedure applies to $[CaSO_4]$ and [NaCl]. When a particle has more than one cation (of Na, Mg, Ca, and K) or more than one anion (S and Cl), the mole number of salts depends on that of each element as follows.

If [Ca] + [Na] + [Mg] + [K] > [S] + [Cl],

$$[CaSO_4] = \frac{[Ca]}{([Ca] + [Na] + [Mg] + [K])} \times [S] ,$$

$$[Na_2SO_4] = \frac{[Na]}{([Ca] + [Na] + [Mg] + [K])} \times [S] .$$

$$[NaCl] = \frac{[Na]}{([Ca] + [Na] + [Mg] + [K])} \times [Cl]$$

$$[Ca\text{-}Cl] = \frac{[Ca]}{([Ca] + [Na] + [Mg] + [K])} \times [Cl]$$

$$[CaCO_3] = [Ca]–[CaSO_4]–[Ca\text{-}Cl]$$

$$[NaX] = [Na]–[Na_2SO_4]–[NaCl].$$

If [Ca] + [Na] + [Mg] + [K] < [S] + [Cl],

$$[CaSO_4] = [Ca] \times \frac{[S]}{[S] + [Cl]} ,$$

$$[Na_2SO_4] = [Na] \times \frac{[S]}{[S] + [Cl]} ,$$

$$[NaCl] = [Na] \times \frac{[Cl]}{[S] + [Cl]} ,$$

$$[Ca\text{-}Cl] = [Ca] \times \frac{[Cl]}{[S] + [Cl]} ,$$

$$[CaCO_3] = 0$$

$$[NaX] = 0.$$

If a particle does not have S and Cl,

$$[Na_2SO_4] = 0$$

$$[CaSO_4] = 0$$

$$[NaCl] = 0$$

$$[Ca\text{-}Cl] = 0$$

$$[CaCO_3] = [Ca]$$

$$[NaX] = [Na].$$

Uncertainty in the mole number was calculated following *Oyabu et al.* [2014]. Variability of the analysis, measured by the coefficient of variation, or CV, was checked. A particle was selected at random. If, for example, it contained Na and S, then we repeatedly (20×) measured its atomic ratios of Na. Then the ratio of the standard deviation to the average value of the 20 measurements (CV_{Na}) was calculated. CV values of the six major elements (Na, Mg, Ca, K, S, and Cl) were obtained in the same way. The average coefficient of variation of these elements was similar to each other, so we used their average value (CV = 0.22). For calculating the mole number of nonvolatile particles, we regarded each particle as an ellipsoid of revolution around the particle major axis, with major and minor axes taken from the particle image observed by SEM. The error of this assumption was obtained by picking 200 particles at random, then measuring the deviation between their actual shadow area and comparing to the idealized ellipse shadow area. As a result, 95% of the particles had areas that differed by less than 20%. The total uncertainty of the mass ratio was 51.0%.

Acknowledgments

We thank many individuals and organizations involved in logistics, drill development, drilling, and ice core processing and analysis in the field. NEEM is directed and organized by the Center of Ice and Climate at the Niels Bohr Institute and U.S. NSF, Office of Polar Programs. It is supported by funding agencies and institutions in Belgium (FNRS-CFB and FWO), Canada (NRCan/GSC), China (CAS), Denmark (FIST), France (IPEV, CNRS/INSU, CEA and ANR), Germany (AWI), Iceland (RannIs), Japan (NIPR), Korea (KOPRI), the Netherlands (NWO/ALW), Sweden (VR), Switzerland (SNF), United Kingdom (NERC), and the USA (U.S. NSF, Office of Polar Programs). We are grateful to T. Karlin of Stockholm University for helping us to set up the sublimation system at Stockholm University, M. Bigler for useful comments and fruitful discussions, D. Leuenberger for fruitful discussions, M. Furusaki for help with SEM-EDS analysis, and J. Nelson for help with revising the manuscript. The paper was significantly improved as a result of comments by M. Legrand of Laboratoire de Glaciologie et Géophysique de l'Environnemt, anonymous reviewers, and the Scientific Editor L. Russell to whom we are greatly indebted. This study was supported by Nordic Centre of Excellence Cryosphere-atmosphere interactions in a changing Arctic climate (CRAICC), by JSPS KAKENHI grants 40370043, 26257201, and 26610147, and by the grant for Joint Research Program of the Institute of Low Temperature Science, Hokkaido University. This work was also supported by the JSPS Institutional Program for Young Researcher Overseas Visits. Inquiries about the data used in the study can be made to the authors. All the data are available through personal communication with the corresponding author (oyabu@lowtem.hokudai.ac.jp).

References

Badens, E., S. Veesler, and R. Boistelle (1999), Crystallization of gypsum from hemihydrate in presence of additives, *J. Cryst. Growth*, *198/199*, 704–709, doi:10.1016/S0022-0248(98)01206-8.

Bigler, M., A. Svensson, E. Kettner, P. Vallenlonga, M. E. Nielsen, and J. P. Steffensen (2011), Optimization of high-resolution continuous flow analysis for transient climate signals in ice cores, *Environ. Sci. Technol.*, *45*, 4483–4489, doi:10.1021/es200118j.

Bory, A. J.-M., P. E. Biscaye, A. M. Piotrowski, and J. P. Steffensen (2003), Regional variability of ice core dust composition and provenance in Greenland, *Geochem. Geophys. Geosyst.*, *4*(12), 1107, doi:10.1029/2003GC000627.
De Angelis, M., J. P. Steffensen, M. Legrand, H. Clausen, and C. Hammer (1997), Primary aerosol (sea salt and soil dust) deposited in Greenland ice during the last climatic cycle: Comparison with east Antarctic records, *J. Geophys. Res.*, *102*(C12), 26,681–26,698, doi:10.1029/97JC01298.
Downs, R. T. (2006), The RRUFF Project: An integrated study of the chemistry, crystallography, Raman and infrared spectroscopy of minerals, Abstracts of the 19th General Meeting of the International Mineralogical Association in Kobe, Japan. O03-13.
Fischer, H., M.-L. Siggaard-Andersen, U. Ruth, R. Röthlisberger, and E. Wolff (2007), Glacial/interglacial changes in mineral dust and sea-salt records in polar ice cores: Sources, transport, and deposition, *Rev. Geophys.*, *45*, RG1002, doi:10.1029/2005RG000192.
Fischer, H., S. Schüpbach, G. Gfeller, M. Bigler, R. Röthlisberger, T. Erhardt, T. F. Stocker, R. Mulvaney, and E. Wolff (2015), Millennial changes in North American wildfire and soil activity over the last glacial cycle, *Nat. Geosci.*, *8*, 723–727.
Fuhrer, K., and M. Legrand (1997), Continental biogenic species in the Greenland Ice Core Project ice core: Tracing back the biomass history of the North American continent, *J. Geophys. Res.*, *102*(C12), 26,735–26,748, doi:10.1029/97JC01299.
Fuhrer, K., A. Neftel, M. Anklin, and V. Maggi (1993), Continuous measurements of hydrogen peroxide, formaldehyde, calcium and ammonium concentrations along the new GRIP ice core from summit, central Greenland, *Atmos. Environ.*, *27A*(12), 1873–1880, doi:10.1016/0960-1686(93)90292-7.
Fuhrer, K., A. Neftel, M. Anklin, T. Staffelbach, and M. Legrand (1996), High-resolution ammonium ice core record covering a complete glacial-interglacial cycle, *J. Geophys. Res.*, *101*(D12), 4147–4164, doi:10.1029/95JD02903.
Gfeller, G., H. Fischer, M. Bigler, S. Schüpbach, D. Leuenberger, and O. Mini (2014), Representativeness of major ions measurements and seasonality derived from NEEM firn cores, *Cryosphere*, *8*, 1855–1870, doi:10.5194/tc-8-1855-2014.
Hammer, C. U., H. B. Clausen, W. Dansgaard, A. Neftel, P. Kristinsdottir, and E. Johnson (1985), Continuous impurity analysis along the Dye 3 deep core, in *Greenland Ice Core: Geophysics, Geochemistry, and the Environment*, edited by C. C. Langway, H. Oeschger, and W. Dansgaard, pp. 90–94, AGU, Washington, D. C.
Hansson, M. (1994), The Renland ice core: A Northern Hemisphere record of aerosol composition over 120,000 years, *Tellus B*, *46*(5), 390–418, doi:10.1034/j.1600-0889.1994.t01-4-00005.x.
Hansson, M., and K. Holmén (2001), High latitude biospheric activity during the last glacial cycle revealed by ammonium variations in Greenland ice cores, *Geophys. Res. Lett.*, *28*(22), 4239–4242, doi:10.1029/2000GL01231.
Hansson, M. E., and E. S. Saltzman (1993), The first Greenland ice core record of methanesulfonate and sulfate over a full glacial cycle, *Geophys. Res. Lett.*, *20*, 1163–1166, doi:10.1029/93GL00910.
Hinds, W. C. (1999), *Aerosol Technology*, 2nd ed., 8 pp., Wiley-Interscience, New York.
Iizuka, Y., S. Horikawa, T. Sakurai, S. Johnson, D. Dahl-Jensen, J. P. Steffensen, and T. Hondoh (2008), A relationship between ion balance and the chemical compounds of salt inclusions found in the Greenland Ice Core Project and Dome Fuji ice cores, *J. Geophys. Res.*, *113*, D07303, doi:10.1029/2007JD009018.
Iizuka, Y., T. Miyake, M. Hirabayashi, T. Suzuki, S. Matoba, H. Motoyama, Y. Fujii, and T. Hondoh (2009), Constituent elements of insoluble and non-volatile particles during the Last Glacial Maximum exhibited in the Dome Fuji (Antarctica) ice core, *J. Glaciol.*, *55*, 552–562, doi:10.3189/002214309788816696.
Iizuka, Y., A. Tsuchimoto, Y. Hoshina, T. Sakurai, M. Hansson, T. Karlin, K. Fujita, F. Nakazawa, H. Motoyama, and S. Fujita (2012a), The rates of sea salt sulfatization in the atmosphere and surface snow of inland Antarctica, *J. Geophys. Res.*, *117*, D04308, doi:10.1029/2011JD016378.
Iizuka, Y., R. Uemura, H. Motoyama, T. Suzuki, T. Miyake, M. Hirabayashi, and T. Hondoh (2012b), Sulphate-climate coupling over the past 300,000 years in inland Antarctica, *Nature*, *490*, 81–84, doi:10.1038/nature11359.
Iizuka, Y., B. Delmonte, I. Oyabu, T. Karlin, V. Maggi, S. Albani, M. Fukui, T. Hondoh, and M. Hansson (2013), Sulphate and chloride aerosols during Holocene and last glacial periods preserved in the Talos Dome Ice Core, a peripheral region of Antarctica, *Tellus B*, *65*, 20197, doi:10.3402/tellusb.v65i0.20197.
Intergovernmental Panel on Climate Change (2007), *Climate Change 2007: The Scientific Basis. Contribution of Working Group I to the Fourth Assessment Report of the Intergovernmental Panel on Climate Change*, edited by S. Solomon et al., Cambridge Univ. Press, Cambridge, U. K., and New York.
Intergovernmental Panel on Climate Change (2013), *Climate Change 2013: The Physical Science Basis. Working Group I Contribution to the IPCC 5th Assessment Report—Changes to the Underlying Scientific/Technical Assessment*, edited by T. Stocker et al., Cambridge Univ. Press, Cambridge, U. K., and New York.
Jonsell, U., M. E. Hansson, M.-L. Siggaard-Andersen, and J. P. Steffensen (2007), Comparison of Northern and Central Greenland ice core records of Methanesulfonate covering the last glacial period, *J. Geophys. Res.*, *112*, D14313, doi:10.1029/2006JD007451.
Kargel, J. S. (1991), Brine volcanism and the interior structures of asteroids and icy satellites, *Icarus*, *94*(2), 368–390.
Kaufmann, P. R., U. Federer, M. A. Hutterli, M. Biglar, S. Schüpbach, U. Ruth, J. Schmitt, and T. F. Stocker (2008), An improved continuous flow analysis system for high-resolution field measurements on ice cores, *Environ. Sci. Technol.*, *42*(21), 8044–8050, doi:10.1021/es8007722.
Kihara, K., T. Hirose, and K. Shinoda (2005), Raman epectra, normal modes and disorder in monoclinic tridymite and its higher temperature orthorhombic modification, *J. Mineral. Petrol. Sci.*, *100*, 91–103, doi:10.2465/jmps.100.91.
Kuramoto, T., K. Goto-Azuma, M. Hirabayashi, T. Miyake, H. Motoyama, D. Dahl-Jensen, and J. P. Steffesen (2011), Seasonal variations of snow chemistry at NEEM, Greenland, *Annal. Glaciol.*, *52*(58), 193–200, doi:10.3189/172756411797252365.
Legrand, M. (1987), Chemistry of Antarctic snow and ice, *J. Phys.*, *48*, 77–86.
Legrand, M. (1995), Atmospheric chemistry changes versus past climate inferred from polar ice cores, in *Aerosol Forcing of Climate*, edited by R. J. Charlson and J. Heintzenberg, pp. 123–151, John Wiley, New York.
Legrand, M., and P. Mayewski (1997), Glaciochemistry of polar ice cores: A review, *Rev. Geophys.*, *35*(3), 219–243, doi:10.1029/96RG03527.
Legrand, M., M. De Angelis, and F. Maupetit (1993), Field investigation of major and minor ions along Summit (Central Greenland) ice cores by ion chromatography, *J. Chromatogr.*, *640*, 251–258, doi:10.1016/0021-9673(93)80188-E.
Legrand, M., C. Hammer, M. De Angelis, J. Savarino, R. Delmas, H. Clausen, and S. J. Johnsen (1997), Sulfur-containing species (methanesulfonate and SO_4) over the last climatic cycle in the Greenland Ice Core Project (central Greenland) ice core, *J. Geophys. Res.*, *102*, 26,663–26,679, doi:10.1029/97JC01436.
Legrand, M. R., and R. J. Delmas (1988a), Soluble impurities in four Antarctic ice cores over the last 30,000 years, *Ann. Glaciol.*, *10*, 116–129.
Legrand, M. R., and R. J. Delmas (1988b), Formation of HCl in the Antarctic atmosphere, *J. Geophys. Res.*, *93*, 7153–7168, doi:10.1029/JD093iD06p07153.
Littot, G. C., R. Mulvaney, R. Röthlisberger, R. Udisti, E. W. Wolff, E. Castellano, M. De Angelis, M. E. Hansson, S. Sommer, and J. P. Steffensen (2002), Comparison of analytical methods used for measuring major ions in the EPICA Dome C (Antarctica) ice core, *Ann. Glaciol.*, *35*, 299–305, doi:10.3189/172756402781817022002.

Liu, T., and Z. Ding (1998), Chinese loess and the paleomonsoon, *Annu. Rev. Earth Planet. Sci.*, *26*, 111–145, doi:10.1146/annurev.earth.26.1.111.

Liu, Y., E. R. Gibson, J. P. Cain, H. Wang, V. H. Grassian, and A. Laskin (2008), Kinetics of heterogeneous reaction of $CaCO_3$ particles with gaseous HNO_3 over a wide range of humidity, *J. Phys. Chem. A*, *112*, 1561–1571.

Maggi, V. (1997), Mineralogy of atmospheric microparticles deposited along the Greenland Ice Core Project ice core, *J. Geophys. Res.*, *102*(C12), 26,725–26,734, doi:10.1029/97JC00613.

Marion, G. (2002), A molal-based model for strong acid chemistry at low temperatures (<200 to 298 K), *Geochim. Cosmochim. Acta*, *66*(14), 2499–2516, doi:10.1016/S0016-7037(02)00857-8.

Mayewski, P. A., et al. (1994), Changes in atmospheric circulation and ocean ice cover over the North Atlantic during the last 41,000 years, *Science*, *263*, 1747–1751, doi:10.1126/science.263.5154.1747.

Meese, D. A., A. J. Gow, R. B. Alley, G. A. Zielinski, P. M. Grootes, M. Ram, K. C. Taylor, P. A. Mayewski, and J. F. Bolzan (1997), The Greenland Ice Sheet Project 2 depth-age scale: Methods and results, *J. Geophys. Res.*, *102*(C12), 26,411–26,423, doi:10.1029/97JC00269.

Montagnat, M., N. Azuma, D. Dahl-Jensen, J. Eichler, S. Fujita, F. Gillet-Chaulet, S. Kipfstuhl, D. Samyn, A. Svensson, and I. Weikusat (2014), Fabric along the NEEM ice core, Greenland, and its comparison with GRIP and NGRIP ice cores, *Cryosphere*, *8*, 1129–1138, doi:10.5194/tc-8-1129-2014.

NEEM community members (2013), Eemian interglacial reconstructed from a Greenland folded ice core, *Nature*, *493*, 489–494, doi:10.1038/nature11789.

Ohno, H., M. Igarashi, and T. Hondoh (2005), Salt inclusions in polar ice core: Location and chemical form of water-soluble impurities, *Earth Planet. Sci. Lett.*, *232*, 171–178, doi:10.1016/j.epsl.2005.01.001.

Ohno, H., M. Igarashi, and T. Hondoh (2006), Characteristics of salt inclusions in polar ice from Dome Fuji, East Antarctica, *Geophys. Res. Lett.*, *33*, L08501, 2006, doi:10.1029/2006GL025774.

Oyabu, I., Y. Iizuka, R. Uemura, T. Miyake, M. Hirabayashi, H. Motoyama, T. Sakurai, T. Suzuki, and T. Hondoh (2014), Chemical compositions of sulfate and chloride salts over the last termination reconstructed from the Dome Fuji ice core, inland Antarctica, *J. Geophys. Res. Atmos.*, *119*, 14,045–14,058, doi:10.1002/2014JD022030.

Petit, J. R., et al. (1999), Climate and atmospheric history of the past 420,000 years from the Vostok ice core, Antarctica, *Nature*, *399*, 429–463, doi:10.1038/20859.

Popovicheva, O., V. Kozlov, E. Kireeva, N. Persianseva, G. Engling, K. Eleftheriadis, E. Diapouli, and D. Saraga (2014), Aerosol in emissions of Siberian biomass burning: Small-scale fire study, *ProScience*, *1*, 405–410, doi:10.14644/dust.2014.066.

Pöschl, U. (2005), Atmospheric aerosols: Composition, transformation, climate and health effects, *Angew. Chem., Int. Ed.*, *44*(46), 7520–7540, doi:10.1002/anie.200501122.

Ram, M., and G. Koenig (1997), Continuous dust concentration profile of pre-Holocene ice from the Greenland Ice Sheet Project 2 ice core: Dust stadials, interstadials, and the Eemian, *J. Geophys. Res.*, *102*(C12), 26,641–26,648, doi:10.1029/96JC03548.

Rasmussen, S. O., et al. (2013), A first chronology for the North Greenland Eemian Ice Drilling (NEEM) ice core, *Clim. Past*, *9*, 2713–2730, doi:10.5194/cp-9-2713-2013.

Rasmussen, S. O., et al. (2014), A stratigraphic framework for abrupt climatic changes during the Last Glacial period based on three synchronized Greenland ice-core records: Refining and extending the INTIMATE event stratigraphy, *Quat. Sci. Rev.*, *106*, 14–28, doi:10.1016/j.quascirev.2014.09.007.

Röthlisberger, R., M. Bigler, M. Hutterli, S. Sommer, and B. Stauffer (2000), Technique for continuous high-resolution analysis of trace substances in firn and ice cores, *Environ. Sci. Technol.*, *34*, 338–342, doi:10.1021/es9907055.

Röthlisberger, R., et al. (2002), Nitrate in Greenland and Antarctic ice cores: A detailed description of post-depositional processes, *Ann. Glaciol.*, *35*, 209–216, doi:10.3189/172756402781817220.

Röthlisberger, R., R. Mulvaney, E. W. Wolff, M. A. Hutterli, M. Bigler, M. de Angelis, M. E. Hansson, J. P. Steffensen, and R. Udisti (2003), Limited dechlorination of sea-salt aerosols during the last glacial period: Evidence from the European Project for Ice Coring in Antarctica (EPICA) Dome C ice core, *J. Geophys. Res.*, *208*(D16), 4256, doi:10.1029/2003JD003604.

Ruth, U., and D. Wagenbach (2003), Continuous record of microparticle concentration and size distribution in the central Greenland NGRIP ice core during the last glacial period, *J. Geophys. Res.*, *108*(D3), 4098, doi:10.1029/2002JD002376.

Ruth, U., M. Bigker, R. Röthlisberger, M.-L. Siggaard-Andersen, S. Kipfstuhk, K. Goto-Azuma, M. Hansson, S. J. Jonsen, H. Lu, and J. P. Steffensen (2007), Ice core evidence for a very tight link between North Atlantic and east Asian glacial climate, *Geophys. Res. Lett.*, *34*, L03706, doi:10.1029/2006GL027876.

Sakurai, T., Y. Iizuka, S. Horikawa, S. Johnsen, D. Dahl-Jensen, J. P. Steffensen, and T. Hondoh (2009), Direct observation of salts as micro-inclusions in the Greenland GRIP ice core, *J. Glaciol.*, *55*, 193, doi:10.3189/002214309790152483.

Sakurai, T., H. Ohno, F. E. Genceli, S. Horikawa, Y. Iizuka, T. Uchida, and T. Hondoh (2010), Magnesium methanesulfonate salt found in the Dome Fuji (Antarctica) ice core, *J. Glaciol.*, *56*(199), 837–842.

Sakurai, T., H. Ohno, S. Horikawa, Y. Iizuka, T. Uchida, K. Hirakawa, and T. Hondoh (2011), The chemical forms of water-soluble microparticles preserved in the Antarctic ice sheet during Termination I, *J. Glaciol.*, *57*(206), 1027–1032, doi:10.3189/002214310794457335.

Shimohara, K., A. Miyamoto, K. Hyakutake, H. Shoji, M. Takata, and S. Kipfstuhl (2003), Cloudy band observations for annual layer counting on the GRIP and NGRIP, Greenland, deep ice core samples, *Mem. Natl. Inst. Polar Res., Spec. Issue*, *57*, 161–167.

Silvente, E., and M. Legrand (1993), Ammonium to sulphate ratio in aerosol and snow of Greenland and Antarctic regions, *Geophys. Res. Lett.*, *20*(8), 687–690, doi:10.1029/93GL00982.

Svensson, A., P. E. Biscaye, and F. E. Grousset (2000), Characterization of late glacial continental dust in the Greenland Ice Core Project ice core, *J. Geophys. Res.*, *105*(D4), 4637–4656, doi:10.1029/1999JD901093.

Svensson, A., S. W. Nielsen, S. Kipfstuhl, S. J. Johnsen, J. P. Steffensen, M. Bigler, U. Ruth, and R. Röthlisberger (2005), Visual stratigraphy of the North Greenland Ice Core Project (North GRIP) ice core during the last glacial period, *J. Geophys. Res.*, *110*, D02108, doi:10.1029/2004JD005134.

Usdowski, E., and M. Dietzel (1998), *Atlas and Data of Solid-Solution Equilibria of Marine Evaporites*, Springer, Berlin.

Warneck, P. (1999), *Chemistry of the Natural Atmosphere*, vol. 71, 2nd ed., edited by R. Dmowska, J. R. Holton, and H. T. Rossby, pp. 388–389, Academic Press, Amsterdam.

Whitby, K. T. (1978), The physical characteristics of sulfur aerosols, *Atmos. Environ.*, *12*, 135–159, doi:10.1016/0004-6981(78)90196-8.

Whitlow, S., P. A. Mayewski, and J. E. Dibb (1992), A comparison of major chemical species seasonal concentration and accumulation at the south pole and summit, Greenland, *Atmos. Environ.*, *26A*, 2045–2054, doi:10.1016/0960-1686(92)90089-4.

Willison, M. J., A. G. Clarke, and E. M. Zeki (1989), Chloride aerosols in central northern England, *Atmos. Environ.*, *23*(10), 2231–2239, doi:10.1016/0004-6981(89)90185-6.

Xingqi, L., H. Dong, J. A. Rech, R. Matsumoto, Y. Bo, and W. Yongbo (2008), Evolution of Chaka Salt Lake in NE China in response to climatic change during the Latest Pleistocene–Holocene, *Quat. Sci. Rev.*, *27*, 867–879, doi:10.1016/j.quascirev.2007.12.006.

Zhang, A., and Y. Iwasaka (2001), Chlorine deposition on dust particles in marine atmosphere, *Geophys. Res. Lett.*, *28*(18), 3613–3616, doi:10.1029/2001GL013333.